

Very High Energy Gamma Astrophysics

A. DE ANGELIS⁽¹⁾⁽²⁾⁽³⁾⁽⁴⁾, O. MANSUTTI⁽¹⁾⁽³⁾, and M. PERSIC⁽²⁾⁽³⁾

⁽¹⁾ *Dipartimento di Fisica, Università di Udine, via delle Scienze 208, I-33100 Udine, Italy*

⁽²⁾ *INAF, Sezione di Trieste, via G.B. Tiepolo 11, I-34143 Trieste, Italy*

⁽³⁾ *INFN, Sezione di Trieste and Gruppo Collegato di Udine, Italy*

⁽⁴⁾ *Instituto Superior Técnico, Av. Rovisco Pais, 1049-001 Lisboa, Portugal*

Summary. — High-energy photons are a powerful probe for astrophysics and for fundamental physics under extreme conditions. During the recent years, our knowledge of the most violent phenomena in the Universe has impressively progressed thanks to the advent of new detectors for high-energy γ -rays. Observation of γ -rays gives an exciting view of the high-energy universe thanks to satellite-based telescopes (AGILE, GLAST) and to ground-based detectors like the Cherenkov telescopes (H.E.S.S. and MAGIC in particular), which recently discovered more than 60 new very-high-energy sources. The progress achieved with the last generation of Cherenkov telescopes is comparable to the one drawn by EGRET with respect to the previous γ -ray satellite detectors. This article reviews the present status of high-energy gamma astrophysics, with emphasis on the recent results and on the experimental developments.

PACS 95.55.Vj – Neutrino, muon, pion, and other elementary particle detectors; cosmic ray detectors.

PACS 95.85.Pw – Gamma-ray.

PACS 96.50.S – Cosmic rays.

| | | |
|-----|--------|---|
| 188 | 1. | Introduction |
| 191 | 2. | Production processes of gamma-rays |
| 191 | 2'1. | Photons from gravitational collapses |
| 195 | 2'2. | Production from self-annihilation of dark matter |
| 197 | 2'3. | Top-down mechanisms |
| 197 | 3. | Propagation of γ -rays |
| 202 | 4. | Detection techniques |
| 202 | 4'1. | Atmospheric transparency and processes of interaction |
| 204 | 4'2. | Satellites |
| 206 | 4'3. | Ground-based detectors |
| 206 | 4'3.1. | EAS detectors |
| 210 | 4'3.2. | Cherenkov telescopes |
| 218 | 4'4. | Resumé |
| 219 | 5. | The emerging HE and VHE gamma-ray sky |

| | | |
|-----|--------|---|
| 219 | 5.1. | Galactic cosmic-ray accelerators |
| 221 | 5.1.1. | Supernova Remnants |
| 221 | 5.1.2. | Pulsars and Pulsar Wind Nebulae |
| 225 | 5.1.3. | Binary systems |
| 225 | 5.1.4. | The centre of the Milky Way |
| 226 | 5.1.5. | Mystery sources and Cygnus region |
| 226 | 5.2. | Extragalactic sources of VHE γ -rays |
| 226 | 5.2.1. | Satellites of the Milky Way |
| 227 | 5.2.2. | Star-forming galaxies |
| 228 | 5.2.3. | Active Galactic Nuclei |
| 234 | 5.2.4. | Gamma-Ray Bursts |
| 237 | 6. | The future |
| 237 | 6.1. | The future of present detectors |
| 238 | 6.2. | The Cherenkov Telescope Array |
| 240 | 6.3. | Large EAS |
| 241 | 7. | Conclusions |
| 242 | | Acknowledgements |
| 242 | | References |

1. – Introduction

A flow of high-energy particles reaches the Earth. About one century ago, two pioneering works by Victor Hess [1] (who for this was awarded the Physics Nobel Prize in 1936), and by Domenico Pacini [2] (who unfortunately died before 1936: his fundamental work is less known, although it was performed at the same time as Hess', independently, and with different techniques) proved that such particles were of extraterrestrial origin: they were thus called *cosmic rays* [3]. Since their energies far exceed the temperatures ordinarily encountered in astronomical objects, cosmic rays are messengers of the non-thermal universe.

Excluding neutrinos, cosmic rays mainly consist of charged particles, such as protons ($\sim 90\%$), helium nuclei ($<10\%$), ionized heavier elements ($<1\%$), and electrons ($<1\%$), while only 0.1%–1% of the total radiation consists of photons with energy >1 MeV; for historical reasons these are called *γ -rays*.

The energy of cosmic rays covers more than 10 orders of magnitude, from tens of MeV up to 10^{20} eV and higher⁽¹⁾. The dependence of the flux on the energy E of the particle can be approximated by a power law

$$\frac{dN}{dE} \propto E^{-\alpha},$$

⁽¹⁾ A theoretical upper limit on the energy of cosmic rays from distant sources exists. This limit was computed in 1966 by Greisen, Kuzmin and Zatsepin [4], and it is called today the GZK cutoff. Protons with energies above a threshold of about 10^{20} eV suffer a resonant interaction with the cosmic microwave background photons to produce pions ($p+\gamma\rightarrow\Delta\rightarrow N+\pi$). This continues until their energy falls below the production threshold. Because of the mean path associated with the interaction, extragalactic cosmic rays from distances larger than 50 Mpc from the Earth and with energies greater than this threshold energy should not be observed on Earth, and there are no known sources within this distance that could produce them. The Auger experiment recently confirmed the existence of the GZK cutoff [5].

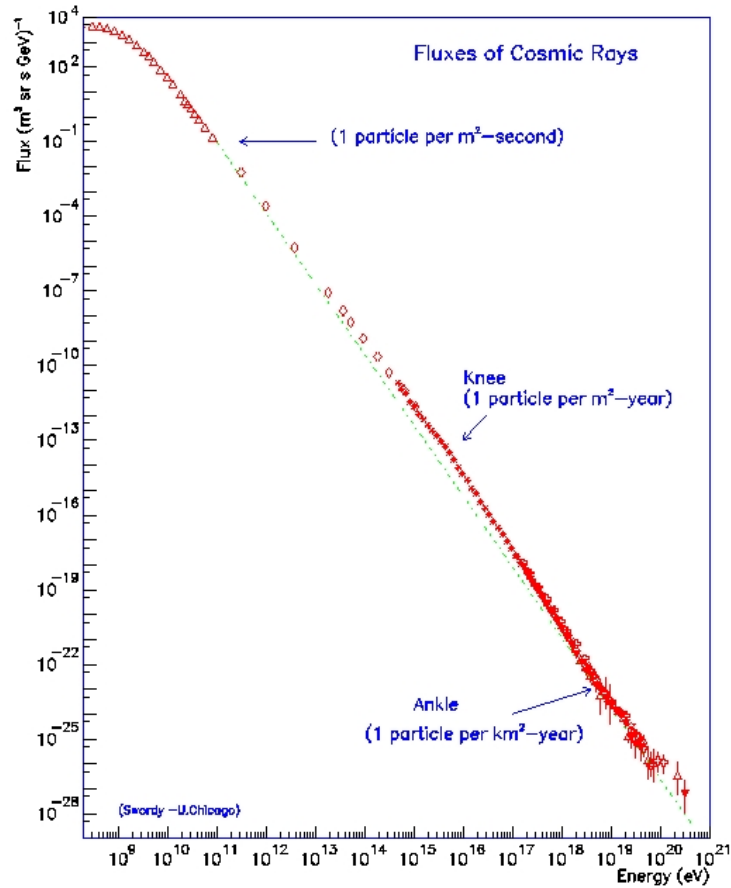


Figure 1. – Energy spectrum of cosmic rays.

where the *spectral index* α has typical values between 2.5 and 3. The energy dependence can be explained in first approximation due to shock acceleration mechanisms [6].

Fig. 1 shows the energy spectrum for cosmic rays. The region around $10^{15.5}$ eV is referred as the “knee”, for its spectral steepening (from a spectral index of about 2.7 to about 3), while the region around $10^{18.5}$ eV, where a spectral flattening occurs, is called the “ankle” of the spectrum. It is generally believed that cosmic rays below the knee have a galactic origin and that they have been confined inside our Galaxy for at least 10^7 years (this can be expected from the value of the magnetic field in the galaxy, which is of the order of $1 \mu\text{G}$) [7]. The particles above 10^{17} eV are believed to be mostly of extragalactic origin, since the galactic magnetic field is not able to trap them in our Galaxy. Recently the Auger collaboration has announced that cosmic rays of energies above 10^{19} eV appear to come from active galactic nuclei (AGN) located within 75 Mpc from our Galaxy [8]. The clustering of arrival directions around the sky positions of those AGNs has enabled to indicate a value of the order of 0.5 nG for the extragalactic magnetic field, at least within a radius of 75 Mpc from the solar system [9].

Although protons are the most abundant component of cosmic rays, their origin is

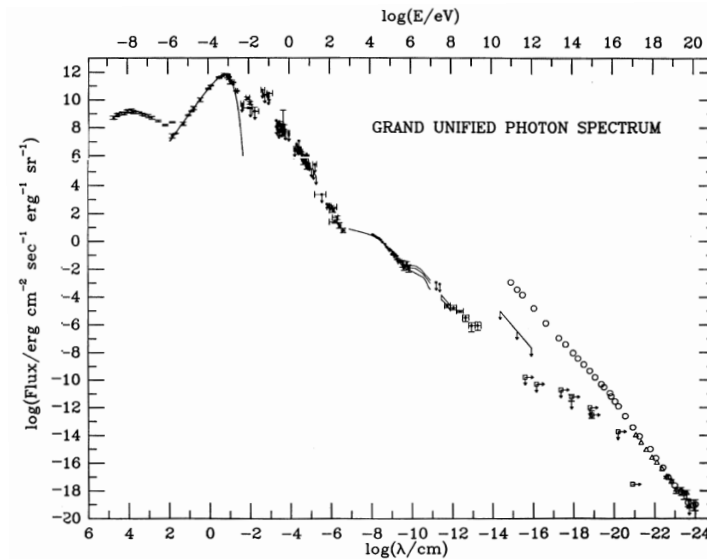


Figure 2. – Flux of diffuse extra-galactic photons [10]. The cosmic microwave radiation peak is visible.

very difficult to determine, since the deflection radius for a proton of energy E crossing a magnetic field of intensity B is:

$$\frac{R}{1 \text{ pc}} \simeq 0.01 \frac{E/1 \text{ TeV}}{B/1 \mu\text{G}}.$$

The directional information of a photon coming from the galactic centre, at a distance of 8 kpc from the Earth, is thus lost below an energy of 300 PeV.

Magnetic fields do not deflect photons, so that they point with very good approximation to the position of the emission source. Since in a hadronic cascade photons can reach some 10% of the energy of the proton originating it, high-energy photons can be a good instrument to study the production of cosmic rays also of hadronic origin.

γ -rays are probably the most interesting part of the spectrum of photon emission from astrophysical sources (Fig. 2). During the recent years, a new window has been opened in the observation of γ -rays above 20 MeV (essentially, the photons above the threshold for pair production, plus some energy phase space), thanks to the availability of new photon detectors coming from technologies typical of experimental particle physics. We shall call such photons, i.e., the photons above 20 MeV, high-energy (HE) γ -rays. Excellent reviews of high energy gamma-ray astrophysics are available; see for example Ref. [11], Ref. [12], Ref. [13], and Ref. [14].

Although arbitrary, the definition of high-energy γ -rays reflects profound astrophysical and experimental arguments:

- the emission is *non-thermal*, and dominated by the conversion of gravitational energy into electromagnetic energy;
- it is impossible to concentrate the photons, which leads to telescopes radically different from the ones dedicated to observations of larger wavelengths;

- large quantity of background events are produced by charged cosmic particles.

High-energy γ -rays today are further classified; such a classification is of course arbitrary. In this paper the energy ranges associated to the definition of low-medium energy, high-energy (HE), very-high-energy (VHE), ultra-high-energy (UHE) and extremely-high-energy (EHE) γ -rays, inspired with small modifications from [15], are the following:

| | |
|-------------------|-------------------|
| low-medium energy | 0.1 MeV - 20 MeV |
| HE | 20 MeV - 30 GeV |
| VHE | 30 GeV - 30 TeV |
| UHE | 30 TeV - 30 PeV |
| EHE | 30 PeV - no limit |

The upper limits on EHE γ -rays come from the heavy reduction of the fluxes as the energy of the observed photons increases (at 30 PeV you expect no more than 1 photon/km² per day from the most powerful sources).

High-energy γ -rays can be detected even if they come from very far distances, since the detection efficiency is good and the mean free path at those energies is large: regions of the sky which are opaque in other energy bands can be transparent to X- and γ -rays, providing us a key to some fundamental physics phenomena.

2. – Production processes of gamma-rays

The source of high-energy photons from astrophysical objects is mainly gravitational energy released by collapses towards a central massive object. In the presence of angular momentum, the dynamics of such a collapse can manifest itself in an accretion disk, with the presence of jets of plasma outflowing the accretion plane. In addition, one could have characteristic photon signals also from annihilation/decay of heavy particles.

At the origin of the production of gamma-rays there is mostly the photon radiation off charged particles, in general electrons. Such a radiation might happen due to

- Bremsstrahlung. An electron in an external field radiates due to bremsstrahlung. The characteristic spectrum of bremsstrahlung is proportional to $1/E$, where E is the energy of the emitted photon. The fractional energy loss due to bremsstrahlung after crossing a distance d is $(1 - e^{-d/X_0})$, where X_0 is called the radiation length of the material. $1/X_0$ is proportional to the density of the material.
- Synchrotron radiation. An electron moving in a magnetic field radiates due a synchrotron radiation strongly beamed into a cone of angle $\alpha \sim m_e/E$, where m_e is the electron mass. Relativistic electrons in a typical galactic magnetic field emit synchrotron radiation at $E_\gamma \simeq 0.05 \left(\frac{E_e}{\text{TeV}}\right)^2 \left(\frac{B}{3\mu\text{G}}\right)$ eV. For ultra-relativistic electrons (typically encountered in astrophysical situations), the emission spectrum is power-law. High-energy synchrotron radiation can only originate in regions of very strong magnetic field, e.g. close to a neutron star surface (where $B \gtrsim 10^{12}$ G).

Alternatively, primary photons can originate from nuclear transition, or decay of π^0 in a hadronic environment.

2.1. Photons from gravitational collapses. – The basic interpretation for the production of high-energy photons from gravitational collapses is the so-called self-synchrotron

Compton (SSC) mechanism. Synchrotron emission from ultra-relativistic electrons accelerated in a magnetic field generates photons with an energy spectrum peaked in the infrared/X-ray range. Such photons in turn interact via Compton scattering with their own parent electron population: since electrons are ultrarelativistic (with a Lorentz factor $\gamma_e \sim 10^{4-5}$), the energy of the upscattered photon gets boosted by a factor $\lesssim \gamma_e^2$.

The upscattering of low-energy photons by collisions with high-energy electrons is the inverse Compton (IC) scattering. This mechanism is very effective for increasing the photon energy (for this reason it is called “inverse”), and is important in regions of high soft-photon energy density and energetic-electron number density.

For a power-law population of relativistic electrons with spectral index q and a black-body population of soft photons at a temperature T , mean photon energies and energy distributions can be calculated for electron energies in the Thomson regime and in the relativistic Klein-Nishina regime:

$$(1) \quad \langle E_\gamma \rangle \simeq \frac{4}{3} \gamma_e^2 \langle \eta \rangle \quad \text{for } \gamma_e \eta \ll m_e c^2 \text{ (Thompson limit)}$$

$$(2) \quad \simeq \frac{1}{2} \langle E_e \rangle \quad \text{for } \gamma_e \eta \gg m_e c^2 \text{ (Klein – Nishina limit)}$$

$$(3) \quad \frac{dN_\gamma}{dE_\gamma} \propto E_\gamma^{-\frac{q+1}{2}} \quad \text{for } \gamma_e \eta \ll m_e c^2 \text{ (Thompson limit)}$$

$$(4) \quad \propto E_\gamma^{-(q+1)} \ln(E_\gamma) \quad \text{for } \gamma_e \eta \gg m_e c^2 \text{ (Klein – Nishina limit)}$$

where where E_γ denotes the scattered photon’s energy, E_e denotes the parent electron’s energy, and η denotes the seed photon’s energy. A useful approximate relation linking the electron’s energy and the Comptonized photon’s energy is given by: $E_\gamma \simeq 6.5 \left(\frac{E_e}{\text{TeV}} \right)^2 \left(\frac{\eta}{\text{meV}} \right) \text{ GeV}$.

The Compton component can peak at GeV–TeV energies; the two characteristic synchrotron and Compton peaks are clearly visible on top of a general E_γ^{-2} dependence. Fig. 3 shows the resulting energy spectrum. This behavior has been verified with high accuracy on the Crab Nebula, a steady VHE gamma emitter in the Milky Way which is often used to calibrate VHE gamma instruments. If in a given region the photons by the synchrotron radiation can be described by a power law with spectral index p , in a first approximation the tails at the highest energies from both the synchrotron and the Compton mechanisms will have a spectral index p .

Alternative and complementary models of VHE emission involve two electron populations, one –primary– accelerated within the jet and the other –secondary– generated by cascades initiated by primary protons/nuclei that had been accelerated in the jet [16]; or a population of extremely energetic protons [17]. In such cases, the energy of the primary protons is expected by the physics of hadronic cascades to be one or two orders of magnitude larger than the energy of gammas, since the dominant mechanism for photon production is the decay of secondary π^0 -mesons into $\gamma\gamma$. The study of γ -rays can thus provide insights on the production of charged cosmic rays.

The case of AGN is particularly relevant. Supermassive black holes of $\sim 10^6$ – 10^9 solar masses (M_\odot) and beyond reside in the cores of most galaxies; their fueling by infalling matter produces a spectacular activity. The black hole is surrounded by an accretion disk and by fast-moving clouds, which emit Doppler-broadened lines ([18, 19]). In about 10% of all AGN, the infalling matter turns on powerful collimated jets that shoot out in opposite directions, likely perpendicular to the disk, at relativistic speeds (see Fig. 4).

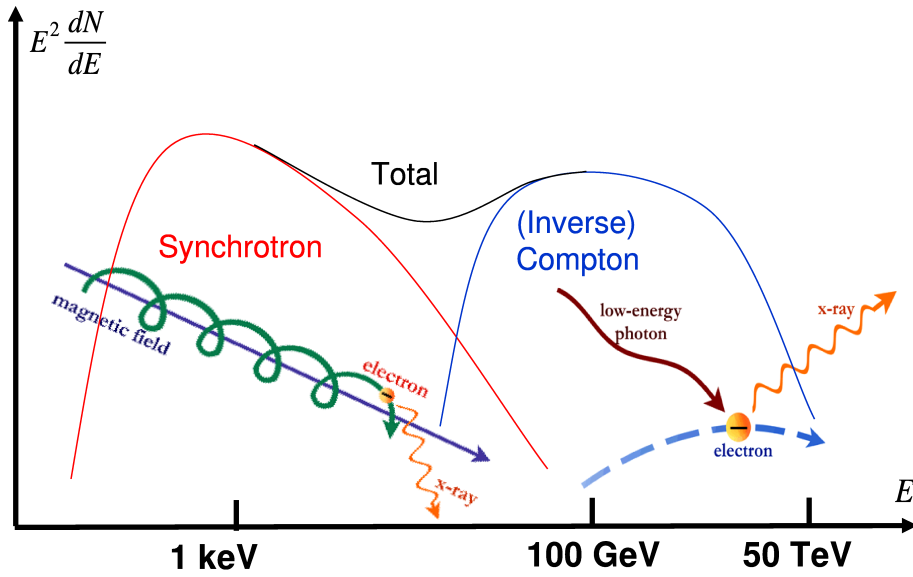


Figure 3. – Differential energy spectrum of photons in the SSC model.

If a relativistic jet is viewed at small angle to its axis the observed jet emission is amplified by relativistic beaming⁽²⁾ and dominates the observed emission; in this case

⁽²⁾ Defining the relativistic Doppler factor as $\delta \equiv [\gamma_j(1 - \beta_j \cos \theta_j)]^{-1}$ (with $\beta_j = v_j/c$ the jet

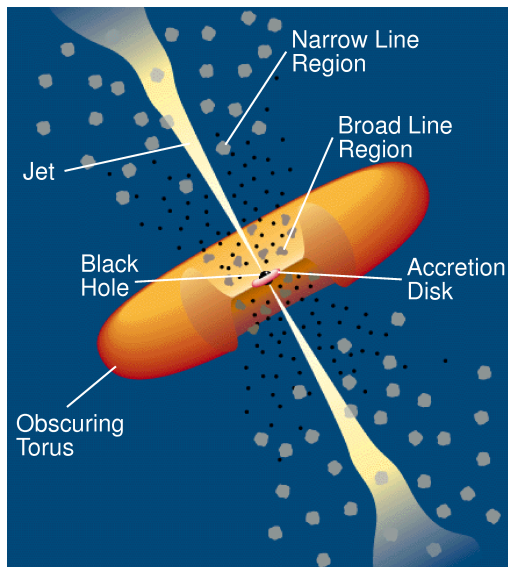


Figure 4. – Schematic diagram for the emission by an AGN [18].

the “quasi-stellar” (quasar) source is called blazar.

Given the compactness of blazars (as suggested by their observed short variability timescales, which can be as low as a couple of minutes for doubling the flux), all GeV/TeV photons would be absorbed through pair-producing $\gamma\gamma$ collisions with target X-ray/IR photons. Beaming ensures the intrinsic radiation density to be much smaller than the observed one, so that γ -ray photons encounter a much lower $\gamma\gamma$ opacity and hence manage to leave the source: reversing the argument, γ -ray detection is a proof of strongly anisotropic (e.g., beamed) emission.

The spectral energy distributions of blazars are generally characterized by two broad humps, peaking at, respectively, infrared/X-ray and GeV-TeV frequencies [20]. Analyses of the spectral energy distribution of blazars [21, 22] have suggested (see Fig. 5) that:

1. higher/lower-luminosity objects have both humps peaking at lower/higher frequencies (they are called, respectively, LBLs and HBLs);
2. the luminosity ratio between the high- and low-frequency humps increases with luminosity;
3. at the highest luminosities the γ -ray output dominates the total luminosity.

Depending on the relative efficiency of the relativistic particles’ cooling through scattering with photon fields that are internal to jet or external to it, the synchrotron and Compton components can also peak at IR/optical and MeV–GeV energies (external-IC, or EIC, scheme, see Ref. [23]). Hybrid SSC/EIC models have also been proposed [22].

The emitting particles are accelerated within the relativistic jets which carry energy from the central black hole outwards [24]. In the SSC framework this process is approximated with a series of relativistically moving homogeneous regions (blobs), where particle acceleration and radiation take place (e.g., Ref. [25]). The X-ray and γ -ray emissions, with their extremely fast and correlated multi-frequency variability, indicate that often a single region dominates the emission; such a region appears to be close to the central engine.

A cornerstone prediction from a pure SSC model is a definite correlation between the yields from synchrotron radiation and from IC during a flare (it would be difficult to accommodate in the theory an “orphan flare”, i.e., a flare in the IC region not accompanied by a flare in the synchrotron region). Evidence of neutrinos in a flare would be a smoking gun for the presence of a hadronic component.

Finally, another very important extragalactic source of γ -rays is given by gamma-ray bursts (GRBs). GRBs are the most luminous events occurring in the universe since the Big Bang. The duration of a GRB is typically a few seconds, but it can range from a few milliseconds to minutes, and the initial burst is usually followed by a longer-lived “afterglow”. Most of them are thought to come from a hypernova, or core-collapse supernova, a cataclysmic event resulting from the internal collapse and violent explosion

speed normalized to the speed of light, $\gamma_j = 1/\sqrt{(1 - \beta_j^2)}$, and θ_j the angle between the jet’s direction and the line of sight), the observed and intrinsic luminosities at a given frequency f are related by $L_f^{\text{obs}} = \delta^p L_f^{\text{em}}$ with $p \sim 2 - 3$, and the variability timescales are related by $\Delta t_{\text{obs}} = \delta^{-1} \Delta t_{\text{em}}$. For $\theta \sim 0^\circ$ and $\delta \sim 2\gamma_j$ the observed luminosity can be amplified by factors $\sim 400 - 10^4$ (for, typically, $\gamma_j \sim 10$ and $p \sim 2 - 3$); whereas $\theta_j \sim 1/\gamma_j$ implies $\delta \sim \gamma_j$, with a luminosity amplification of $\sim 10^2 - 10^3$.

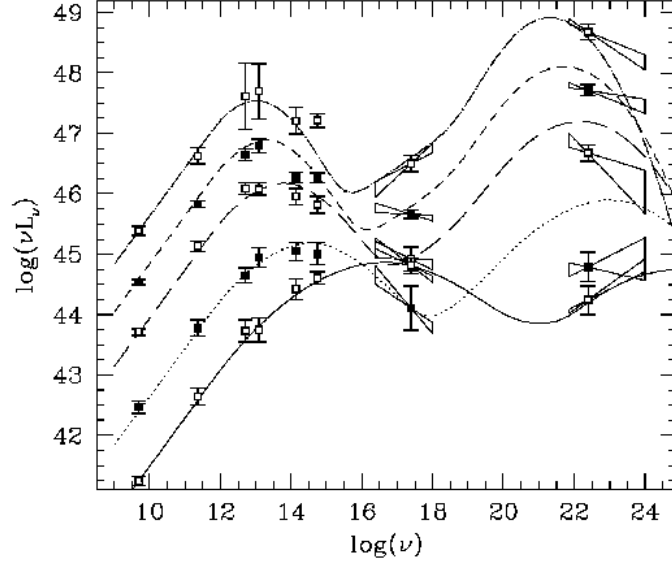


Figure 5. – The active galactic nuclei sequence [21].

of a massive star (the mass of the star needs to be at least 8 times the solar mass to undergo this process). There is a prevailing consensus that the basic mechanism of GRB emission is an expanding relativistic fireball [26, 27, 28], with the beamed radiation due to internal/external shocks (prompt/afterglow phase, respectively).

In the fireball shock framework, several models have predicted VHE emission during both the prompt and afterglow phases of the GRB (e.g., Ref. [29]). This can occur as a result of electron self-IC emission from the internal shock or the external forward/reverse shock. Seed photons can be produced locally (through synchrotron, or be the leftover of the initial radiation content responsible for the acceleration of the fireball) or can be produced in, e.g., the shell of a previously exploded supernova. In the latter case, the photons emitted by the supernova may also act as targets for the $\gamma\gamma$ absorption, and in this case the VHE emission could be severely dimmed. If the emission processes are indeed synchrotron and IC, then a blazar-like spectral energy distribution is predicted, with a double-peak shape extending into the VHE band. In such theoretical freedom, VHE observations of GRBs could help constraining GRB models.

2.2. Production from self-annihilation of dark matter. – Evidence for the departure of cosmological motions from the predictions of Newtonian dynamics based on visible matter, interpreted as due to the presence of dark matter, is well established – from galaxy scales (e.g., [30]) to galaxy-cluster scales (e.g., [31]) to cosmological scales (e.g., [32]).

Dark matter particle candidates should be weakly interacting with ordinary matter (and hence neutral), otherwise they would have been already found. The theoretically favored ones are heavier than the proton, and they are called weakly interacting massive particles (WIMPs); the present experimental limits from accelerators indicate a minimum mass of about 50 GeV [33]. WIMPs should be long-lived enough to have survived from their decoupling from radiation in the early universe into the present epoch.

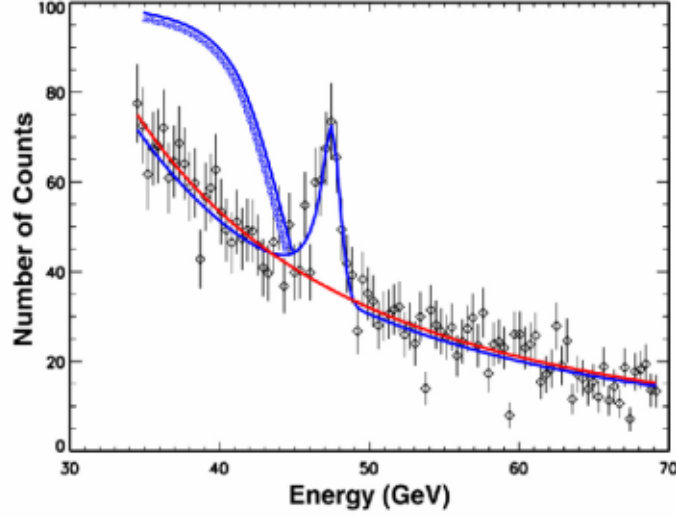


Figure 6. – Simulated signals of the WIMPs self-annihilation: a narrow peak or a continuum below the mass of the WIMP [34].

The main field of research for dark matter in the γ -ray energy range is related to the detection of photons emitted by the self-annihilation of WIMPs. In particular, in supersymmetric models the lightest supersymmetric neutral particle, the neutralino, is predicted to be a Majorana particle, and is thus a natural candidate for such a WIMP.

The self-annihilation of a heavy WIMP χ can generate photons (Fig. 6) in three main ways:

- a) directly via annihilation into a photon pair ($\chi\chi \rightarrow \gamma\gamma$) or into a photon - Z -boson pair ($\chi\chi \rightarrow \gamma Z$) with $E_\gamma = m_\chi$ or $E_\gamma = (m_\chi - m_Z)^2/(4m_\chi)$ respectively; these processes give a clear signature at high energies, being the energy monochromatic, but the process is suppressed at one loop, so the flux is expected to be very faint;
- b) via annihilation into a quark pair which produces jets emitting in turn a large number of γ photons ($qq \rightarrow jets \rightarrow many\ photons$); this process produces a continuum of gammas with energies below the WIMP mass; the flux can be large but the signature might be difficult to detect;
- c) via internal bremsstrahlung [35]; also in this case one has an excess of low energy gammas with respect to a background which is not so well known.

The γ -ray flux from the annihilation of dark matter particles of mass m_{DM} can be expressed as the product of a particle physics component times an astrophysics component:

$$(5) \quad \frac{dN}{dE} = \frac{1}{4\pi} \underbrace{\frac{\langle\sigma v\rangle}{m_{DM}^2} \frac{dN_\gamma}{dE}}_{\text{Particle Physics}} \times \underbrace{\int_{\Delta\Omega-l.o.s.} dl(\Omega)\rho_{DM}^2}_{\text{Astrophysics}} .$$

The particle physics factor contains $\langle\sigma v\rangle$, the velocity-weighted annihilation cross section (there is indeed a possible component from cosmology in v), and dN_γ/dE , the differential γ -ray spectrum summed over the final states with their corresponding branching ratios. The astrophysical part corresponds to the squared density of the dark matter distribution integrated over line of sight (*l.o.s.*) in the observed solid angle.

It is clear that the expected flux of photons from dark matter annihilations, and thus its detectability, depends crucially on the knowledge of the annihilation cross section σ (which even within SUSY has uncertainties of one-two orders of magnitude for a given WIMP mass) and of ρ_{DM} , which is even more uncertain, and enters in the calculation squared. A cuspy dark matter profile, or even the presence of local clumps, could make the detection easier by enhancing ρ_{DM} . The experimental data about the centre of the Galaxy (rotation curves, microlensing, etc.) give however presently no evidence for a cuspy dark matter density profile, but the issue is still debated.

The targets for dark matter searches should be not extended, with the highest density, with no associated astrophysical sources, and close by to us, and possibly with some indication of small luminosity/mass ratio from the stellar dynamics.

The galactic centre is at a distance of about 8 kpc from the Earth. A black hole of about 3.6×10^6 solar masses, Sgr A*, lies there. Because of its proximity, this region might be the best candidate for indirect searches of dark matter. Unfortunately, there are other astrophysical γ -ray sources in the field of view (e.g., the supernova remnant Sgr A East) and the halo core radius makes it an extended rather than a point-like source (see Fig. 7).

Since distance dilution of the signal hinders detection, galaxies candidate for indirect dark matter detection should be chosen among nearby objects. The best observational targets for dark matter detection outside the Galaxy are the Milky Way's dwarf spheroidal satellite galaxies (e.g., Draco, Sculptor, Fornax, Carina, Sextans, Ursa Minor). For all of them (e.g., Draco), there is observational evidence of a mass excess with respect to what can be estimated from luminous objects, i.e., a high M/L ratio.

2'3. Top-down mechanisms. – Finally, some gamma-ray emission could originate in decays of exotic particles of very large mass possibly produced in the early Universe. Such long-lived heavy particles are predicted in many models (e.g., technicolor models or the R-parity - violating SUSY model), and the energy distribution of particles coming from their decay should be radically different from what predicted by the standard emission models from astrophysical sources [34].

3. – Propagation of γ -rays

Electron-positron (e^-e^+) pair production in the interaction of beam photons off extragalactic background photons is a source of opacity of the Universe to γ -rays whenever the corresponding photon mean free path (Fig. 8) is smaller than the source distance.

The dominant process for the absorption is the pair-creation process $\gamma + \gamma_{\text{background}} \rightarrow e^+ + e^-$, for which the cross-section is described by the Bethe-Heitler formula [38]:

$$(6) \quad \sigma(E, \epsilon) \simeq 1.25 \cdot 10^{-25} (1 - \beta^2) \cdot \left[2\beta(\beta^2 - 2) + (3 - \beta^4) \ln \left(\frac{1 + \beta}{1 - \beta} \right) \right] \text{cm}^2$$

where $\beta = \sqrt{1 - \frac{(m_e c^2)^2}{E \epsilon}}$, m_e being the value of the electron mass, E is the energy of the

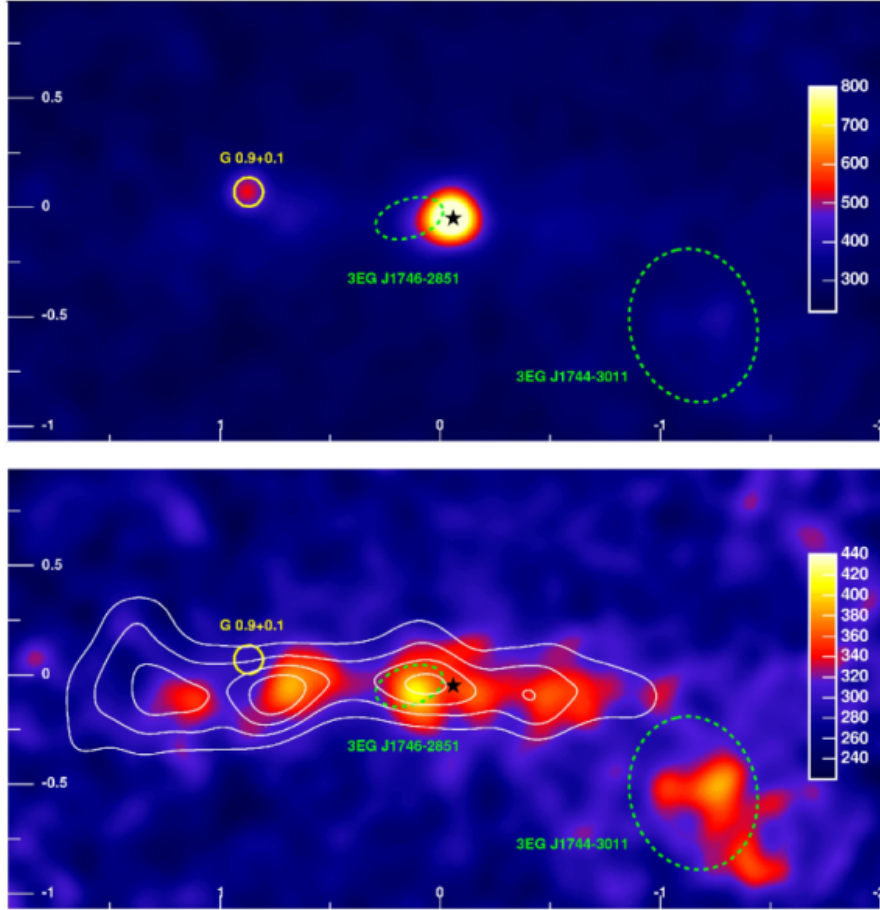


Figure 7. – Image of the galactic centre by the H.E.S.S. telescope [36]. Upper panel: point-like γ -ray sources at the galactic centre; lower panel: the galactic centre in the γ -rays after subtraction of the two point-like sources: an extended source of γ -rays shows up.

(hard) incident photon and ϵ is the energy of the (soft) background photon. Notice that only QED, relativity and cosmology arguments are involved in the previous formula.

The cross section in Eq. 6 is maximized when $\epsilon \simeq \frac{500 \text{ GeV}}{E}$ eV. Hence if $E = 1 \text{ TeV}$ the interaction cross section is maximal if $\epsilon \simeq 0.5 \text{ eV}$ (corresponding to a near-infrared soft photon). In general, for very high energy photons the $\gamma\gamma \rightarrow e^+ + e^-$ interaction becomes important with optical/infrared photons, whereas the interaction with the cosmic microwave background becomes dominant at $E \sim 1 \text{ PeV}$. Therefore, the background component relevant for interaction with VHE photons is the optical/infrared background radiation. This is called extragalactic background light (EBL) [40].

The EBL consists of the sum of starlight emitted by galaxies throughout their whole cosmic history, plus possible additional contributions, like, e.g., light from hypothetical first stars that formed before galaxies were assembled. Therefore, in principle the EBL contains important information both the evolution of baryonic components of galaxies

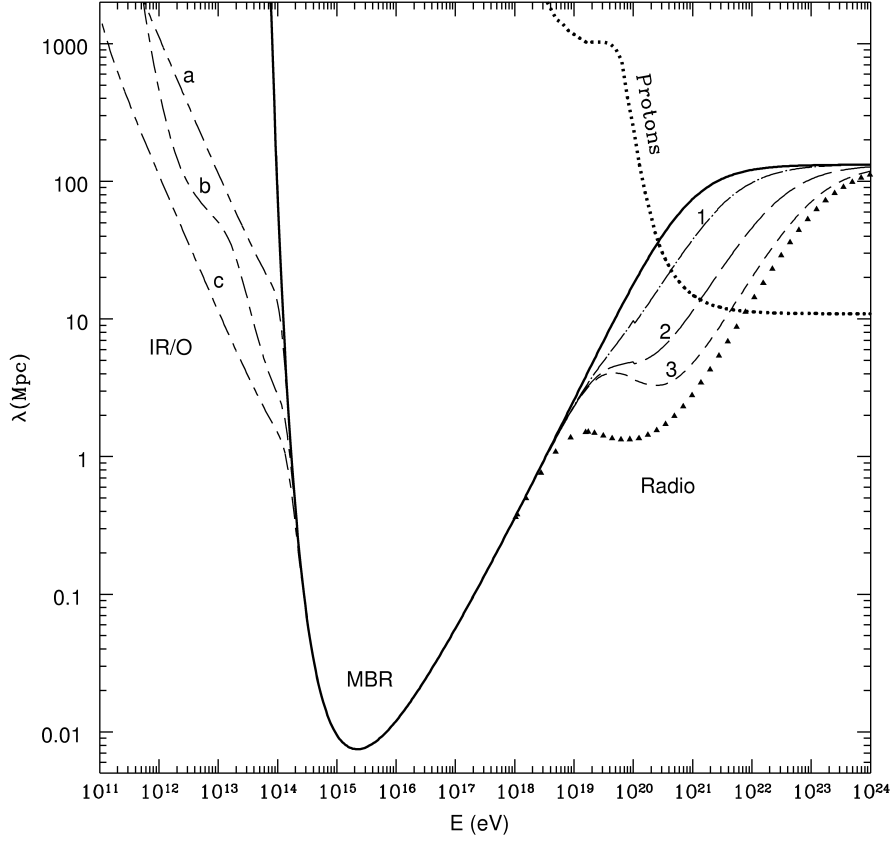


Figure 8. – Mean free path as a function of the photon energy [37].

and the structure of the Universe in the pre-galactic era.

The attenuation suffered by observed VHE spectra can thus be used to derive constraints on the EBL density [41]. First limits on the EBL were obtained in Ref. [42], while recent determinations from the detection of distant VHE sources are reported in [43, 44]. Fig. 9 shows the estimated photon number density of the background photons as composed by the radio background, the cosmic microwave background, and the infrared/optical/ultraviolet background (EBL).

Specifically, the probability for a photon of observed energy E to survive absorption along its path from its source at redshift z to the observer plays the role of an attenuation factor for the radiation flux, and it is usually expressed in the form:

$$(7) \quad e^{-\tau(E,z)}.$$

The coefficient $\tau(E, z)$ is called *optical depth*.

To compute the optical depth of a photon as a function of its observed energy E and the redshift z of its emission one has to take into account the fact that the energy E

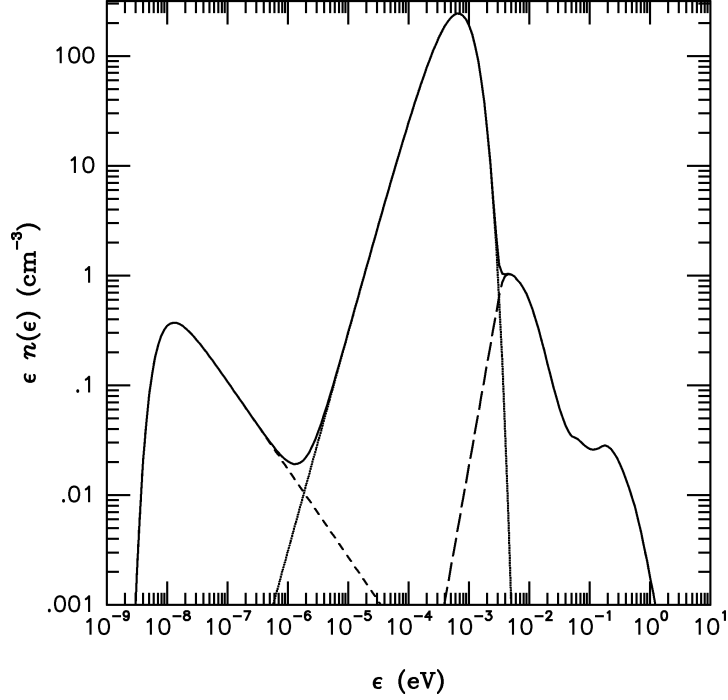


Figure 9. – Photon number density of the intergalactic radiation field at $z = 0$ as developed by Lee [39], composed by the radio background (short dashed line), the cosmic microwave background (dense dotted line), and the infrared/optical/ultraviolet background (EBL) (long dashed line).

of a photon scales with the redshift z as $(1+z)$ [45]; thus when using Eq. 6 we must treat the energies as function of z and evolve $\sigma(E(z), \epsilon(z), \theta)$ for $E(z) = (1+z)E$ and $\epsilon(z) = (1+z)\epsilon$, where E and ϵ are the energies at redshift $z = 0$. The optical depth is then computed [40] by convolving the photon number density of the background photon field with the cross section between the incident γ -ray and the background target photons, and integrating the result over the distance, the scattering angle and the energy of the (redshifted) background photon:

$$(8) \quad \tau(E, z) = \int_0^z dl(z) \int_{-1}^1 d \cos \theta \frac{1 - \cos \theta}{2} \int_{\frac{2(m_e c^2)^2}{E(1 - \cos \theta)}}^{\infty} d\epsilon(z) n_\epsilon(\epsilon(z), z) \sigma(E(z), \epsilon(z), \theta)$$

where θ is the scattering angle, $n_\epsilon(\epsilon(z), z)$ is the density for photons of energy $\epsilon(z)$ at the redshift z , and $l(z) = c dt(z)$ is the distance as a function of the redshift, defined by [46]

$$(9) \quad \frac{dl}{dz} = \frac{c}{H_0} \frac{1}{(1+z) [(1+z)^2 (\Omega_M z + 1) - \Omega_\Lambda z(z+2)]^{\frac{1}{2}}}.$$

In the last formula H_0 is the Hubble constant, Ω_M is the matter density (in units of the critical density, ρ_c) and Ω_Λ is the “dark energy” density (in units of ρ_c); therefore,

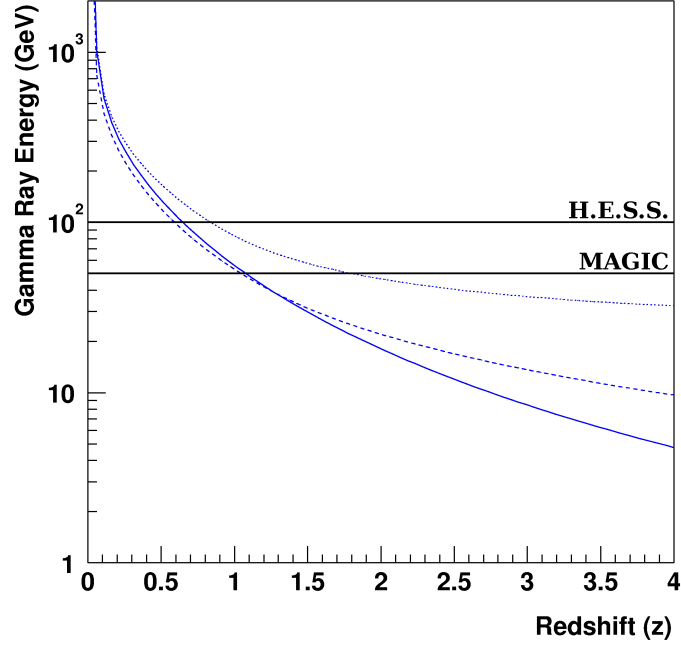


Figure 10. – Gamma-ray horizon compared with the lower energy limit of some gamma detectors: the MAGIC and H.E.S.S. telescopes; the curves of the photon energy versus horizon are computed for different background evolution models by Blanch & Martinez in the second citation in Ref. [47].

since the optical depth depends also on the cosmological parameters, its determination constrains the values of the cosmological parameters [47] if the cosmological emission of galaxies is known.

The energy dependence of τ leads to appreciable modifications of the observed source spectrum (with respect to the spectrum at emission) even for small differences in τ , due to the exponential dependence described in Eq. (7). Since the optical depth (and consequently the absorption coefficient) increases with energy, the observed flux results steeper than the emitted one.

The *horizon* (e.g. Ref. [47, 48]) or *attenuation edge* (e.g. Ref. [49]) for a photon of energy E is defined as the distance corresponding to the redshift z for which $\tau(E, z) = 1$, that gives an attenuation by a factor $1/e$ (see Fig. 10).

Other interactions than the one just described might change our picture of the attenuation of γ -rays, and they are presently subject of thorough studies, since the present data on the absorption of photons are hardly compatible with the pure QED picture. For example, γ -rays might interact with (possibly quintessential) very light axion-like particles, which might change the absorption length [50, 51]. In particular, in the DARMA model [51], such contribution might enhance the photon flux via a regeneration mechanism (see Fig. 11). Such an interaction would be mediated by the (intergalactic) magnetic fields [9]. A similar mechanism invokes the conversion of photons into axion-like particles at the emission source [52].

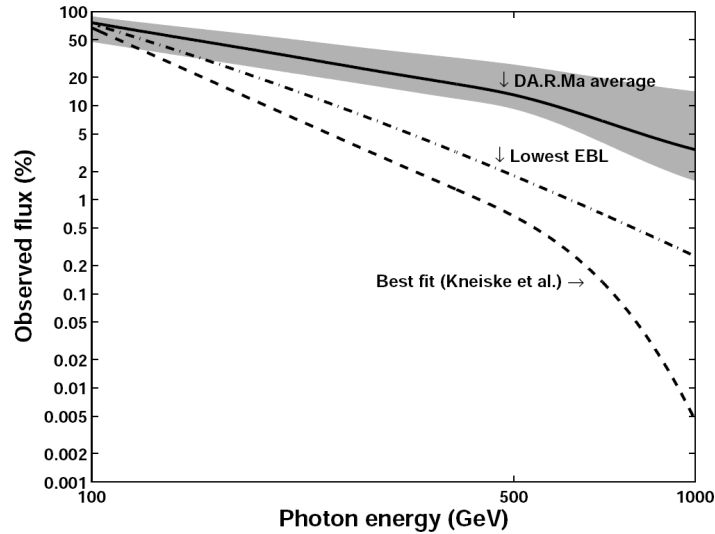


Figure 11. – The two lowest lines give the fraction of photons surviving from a source at the same distance of 3C 279 without the oscillation mechanism, for the “best-fit model” of EBL (dashed line) and for the minimum EBL density compatible with cosmology [53]. The solid line represents the prediction in the DARMA model [51], with an uncertainty represented by the gray band.

Finally, mechanisms in which the absorption is changed through violation of the Lorentz invariance as in Ref. [54] are also under test; such models are particularly appealing within scenarios inspired to quantum gravity [55].

4. – Detection techniques

The detection of high-energy photons is complicated by the absorption by the atmosphere, and by the faintness of the signal, in particular when compared to the corresponding charged particles of similar energy.

4.1. Atmospheric transparency and processes of interaction. – Photons above the ultraviolet (UV) region are shielded by the Earth’s atmosphere (see Fig. 12).

Photons interact with matter mostly due to the Compton mechanism and to the photoelectric effect at energies up to about 20 MeV, while e^+e^- pair production dominates above about 20 MeV. Above about 50 GeV the production of atmospheric showers takes place, dominated by the pair production and the bremsstrahlung mechanisms: an energetic photon scatters on an atmospheric nucleus and produces a pair, which emits secondary photons via bremsstrahlung; such photons produce in turn a e^+e^- pair, and so on, giving rise to a shower of charged particles and photons. The process is described ex. in [57, 58].

The longitudinal development of typical photon-induced extensive air showers is shown in Fig. 13 for different values of the primary energies. The maximum shower

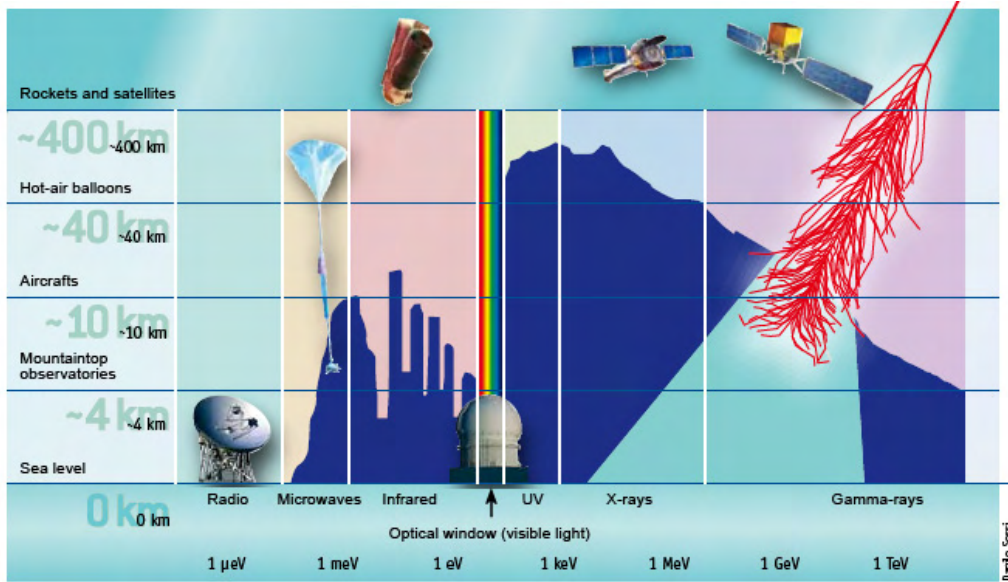


Figure 12. – Transparency of the atmosphere for different photon energies and possible detection techniques [56].

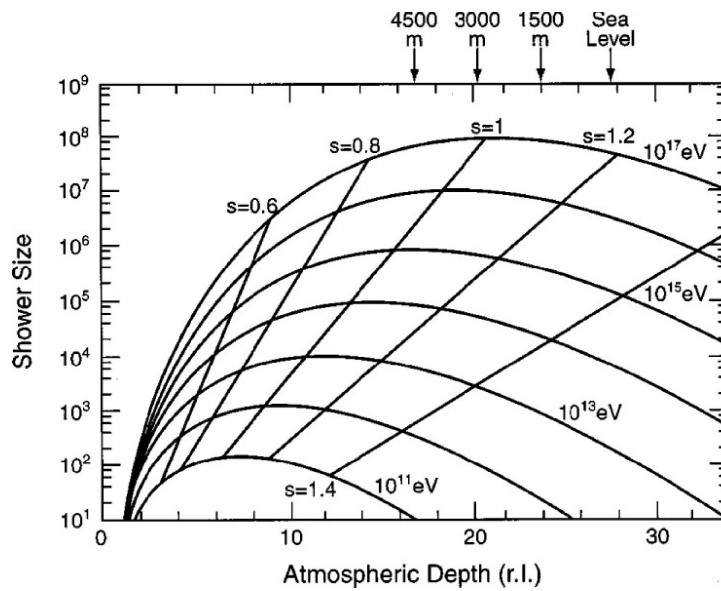


Figure 13. – Longitudinal shower development [12]. The parameter s describes the shower age, being 0 at the first interaction, 1 at the maximum and 2 at the death [57].

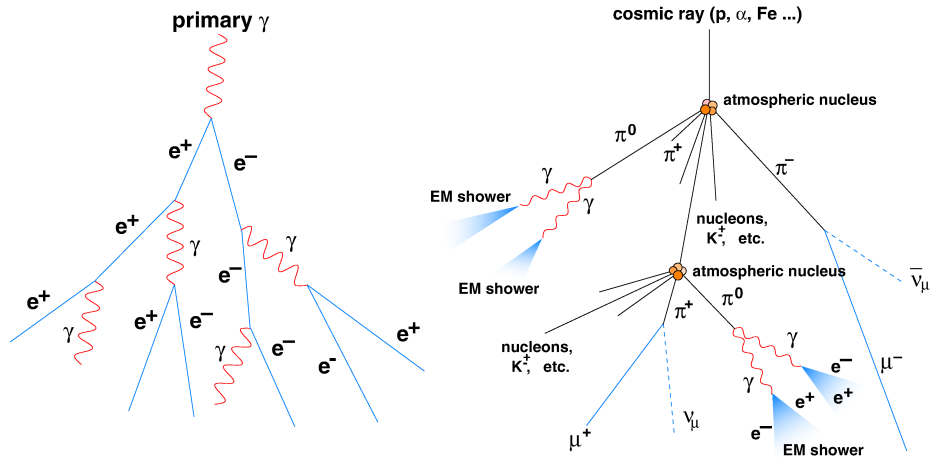


Figure 14. – Schematic representation of two atmospheric showers initiated by a photon (left) or by a cosmic ray (right) [59].

size occurs approximately $\ln(E/\epsilon_0)$ radiation lengths⁽³⁾ into the atmosphere, generally well above ground (the critical energy ϵ_0 , about 80 MeV in air, is the energy at which the ionization energy loss starts dominating the energy loss by bremsstrahlung). Anyway, a large number of shower particles may reach the ground, especially at mountain altitudes.

The dominant high-energy hadrons, protons and nuclei, also interact high in the atmosphere. The process characterizing hadronic showers is not dissimilar (Fig. 14). The hadronic interaction length in air is about 61 g/cm² for protons, being shorter for heavier nuclei. The transverse development of hadronic showers is in general wider than for electromagnetic showers, and fluctuations are larger.

At sea level the thickness of the atmosphere corresponds to about 28 radiation lengths. This means that only satellite-based detectors can detect primary X/ γ -rays. Since the fluxes of high-energy photons are low and decrease rapidly with increasing energy, VHE and UHE gammas can be detected only from the atmospheric showers they produce, i.e., by means of ground-based detectors; such detectors should be placed at high altitudes, where atmospheric dimming is lower.

Let us now examine the characteristics of the satellite-based and ground-based detectors for high-energy photons.

4.2. Satellites. – Main figures of merit for a satellite-borne detector are its effective area (i.e., the product of the area times the detection efficiency), the energy resolution, the space or angular resolution (called as well point-spread function, or PSF), and the time resolution. Satellite HE gamma telescopes such as EGRET, AGILE and GLAST (Fig. 15) detect the primary photons at energies lower than ground-based telescopes. They have a small effective area, of order of 1 m², which yields a low sensitivity. They have a large duty cycle, since they are not constrained by night operation, and they suffer

⁽³⁾ The radiation length X_0 is both the mean distance over which a high-energy electron loses all but $1/e$ of its energy by radiation, and $7/9$ of the mean free path for pair production by a high-energy photon. The radiation length for air is about 37 g/cm².

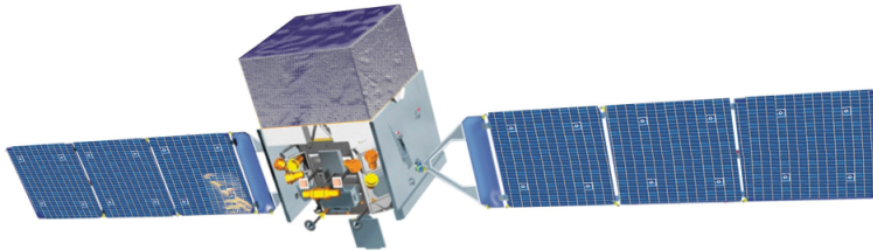


Figure 15. – Image of the GLAST satellite [60].

a low rate of background events, but they have a large cost.

The technology of AGILE and GLAST has been inherited from the EGRET instrument (Fig. 16), operational in 1991–2000 on the Compton Gamma-Ray Observatory. The direction of an incident photon is mostly determined by the geometry of its conversion into an e^+e^- pair in foils of heavy materials which compose the instrument, and detected by planes of silicon detectors. The presence of an anticoincidence apparatus realizes a veto against unwanted incoming charged particles. The angular resolution of these telescopes is limited by the opening angle of the e^+e^- pair, approximately $m_e/E \ln(E/m_e)$, and especially by the effect of multiple scattering.

To achieve a good energy resolution, in this kind of detectors a calorimeter in the bottom of the tracker is possibly used, depending on the weight that the payload is planned to comply with. Due to weight limitations, however, it is difficult to fit in a calorimeter that completely holds the showers; this leakage downgrades the energy resolution. Since at low energies the multiple scattering is the dominant process, the optimal detector design is a tradeoff between small radiation length (which decreases

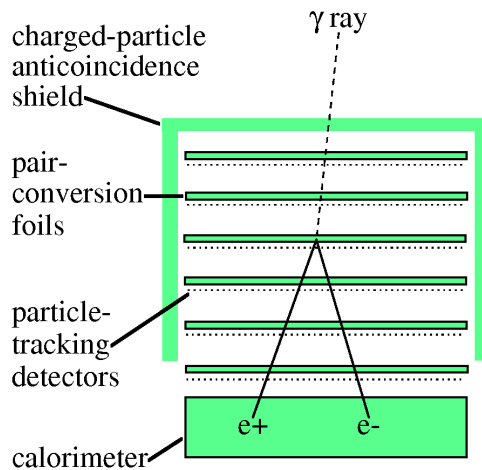


Figure 16. – Pair-production in the typical structure of a satellite detector after an incident γ -ray enters the telescope [61].

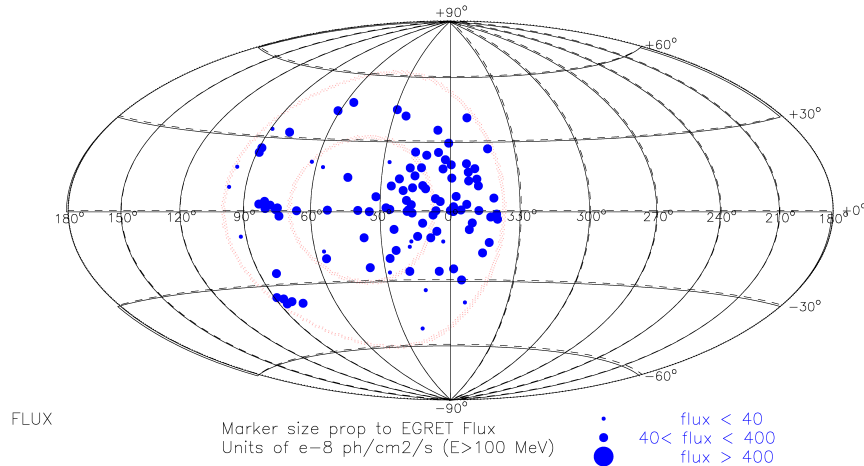


Figure 17. – Example of a region of space explored by AGILE in a single pointing; the field of view (FoV) is indicated [62].

the conversion efficiency) and large number of samplings (which increases the power consumption, limited by the problems of heat dissipation in space).

AGILE is a completely Italian satellite launched in April 2007. Its structure is very similar to GLAST, but its effective area is about one order of magnitude smaller. The physics runs of AGILE (see Fig. 17) started on September 1st, 2007, but many remarkable physics results were observed already during commissioning. Several sources, some of which new, have already been found at >1 GeV.

The GLAST observatory, launched in June 2008, is composed by the spacecraft and by two instruments: the Large Area Telescope (LAT) and the GLAST Burst Monitor (GBM). The two instruments are integrated and they work as a single observatory. The structure of the LAT consists mainly in a tracker, an anticoincidence apparatus and a calorimeter (see Fig. 18). Its energy range goes from 20 MeV to about 300 GeV, while the energy range explored by the GMB is 10 keV – 25 MeV. The GLAST LAT outperforms EGRET by two orders of magnitude thanks to its effective area that approaches 1 m^2 (to be compared to 0.15 m^2 from EGRET) and its time resolution of $10 \mu\text{s}$; a comparison is shown in Fig. 19. Fig. 20 shows a simulation of the HE γ -ray sky emerging from one year of scanning-mode observation by GLAST.

4.3. Ground-based detectors. – Ground-based VHE telescopes such as MILAGRO, ARGO, CANGAROO, H.E.S.S., MAGIC and VERITAS detect the secondary particles of the atmospheric showers produced by primary photons and cosmic rays of energy higher than the primaries observed by satellites. The two kinds of detectors are complementary (see Fig. 2). Such ground-based detectors have a huge effective area, so their sensitivity is high; they detect a huge amount of background events, and they have low cost.

There are two main classes of ground based HE gamma detectors: the Extensive Air Shower arrays (EAS) and the Cherenkov telescopes (see Fig. 21).

4.3.1. EAS detectors. The EAS detectors, such as MILAGRO and ARGO, are made by a large array of detectors sensitive to charged secondary particles generated by the



Figure 18. – On the first row, the two GLAST instruments: the Large Area Telescope (LAT) and the GLAST Burst Monitor (GBM) [63]. On the second row, a picture of the GLAST satellite [64]. On the third row, the first gamma conversion detected by GLAST [60].

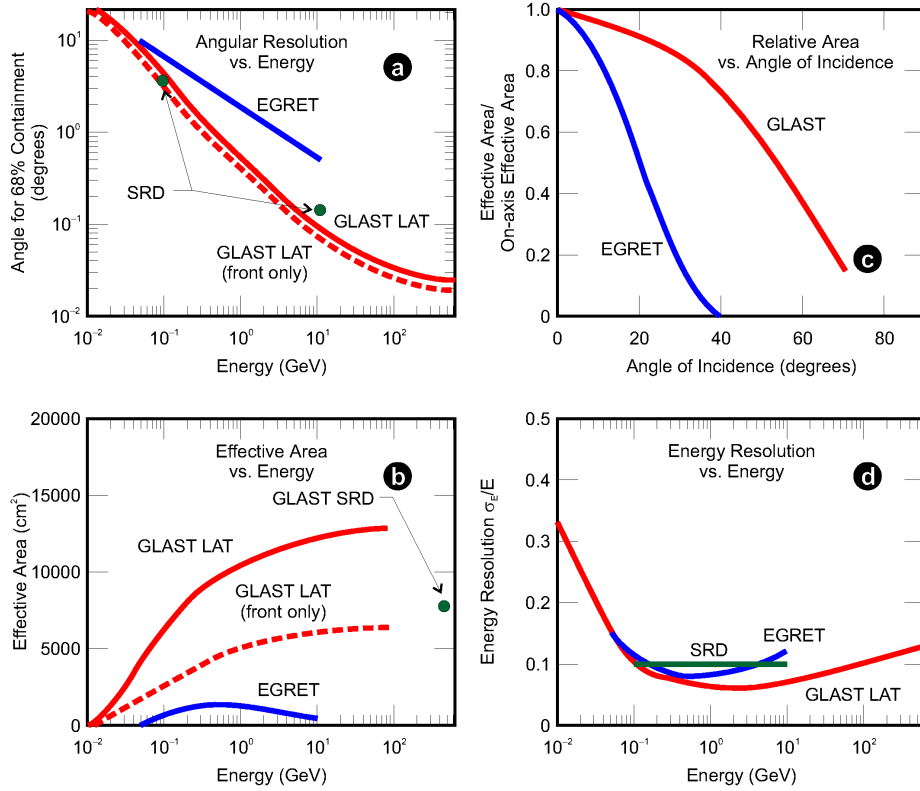


Figure 19. – GLAST LAT performance compared with EGRET [65].

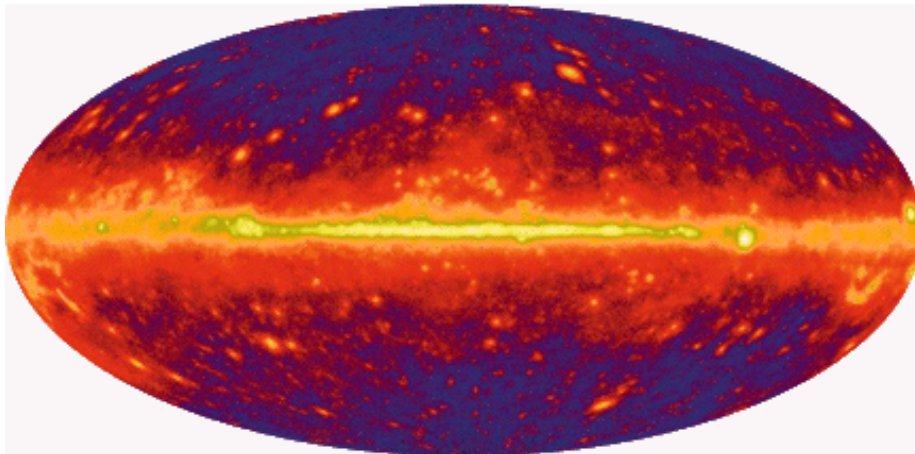


Figure 20. – One-year simulation of the sources that GLAST will detect [60]; the red color corresponds to photons at an energy in the range 0.1 – 0.4 GeV; green corresponds to the energy range 0.4 – 1.6 GeV and blue to more than 1.6 GeV.

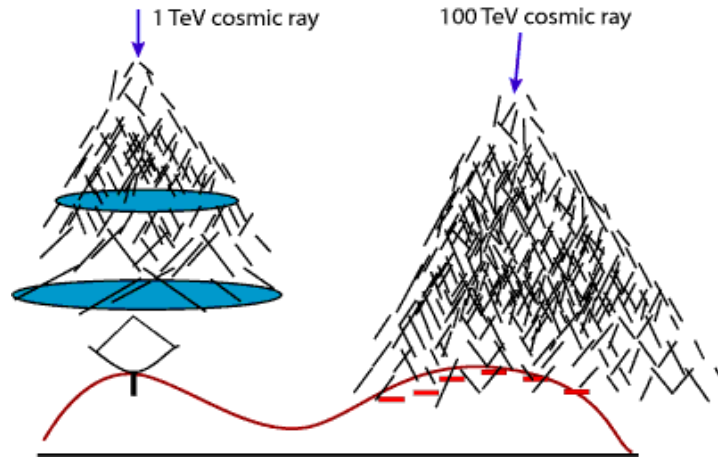


Figure 21. – Sketch of the operation of Cherenkov telescopes and of EAS [66].

atmospheric showers. They have high duty cycle and a large FoV, but a low sensitivity. Since the maximum of a photon-initiated shower at 1 TeV typically occurs at 8 km a.s.l., the energy threshold of such detectors is rather large.

Direct sampling of the charged particles in the shower can be achieved:

- Either by using an array of sparse scintillator-based detectors, as for example in the Tibet AS instrument (located at 4100 m a.s.l. to reduce the threshold). For an energy of 100 TeV there are about 50 000 electrons at mountain-top altitudes, so sampling is possible;
- Or by effective covering of the ground to ensure efficient collection and hence lower energy threshold.
 - The ARGO-YBJ detector (see Fig. 22, [67]) at the Tibet site follows this approach. It is made of an array of resistive plate counters. Its energy threshold lies in the 0.5 TeV-1 TeV range. The first results show that ARGO can detect the Crab Nebula with a significance of about 5 standard deviations (σ) in 50 days of observation.
 - MILAGRO (see Fig. 23) is a water-Cherenkov based instrument near Los Alamos (about 2600 m altitude). It is made of photomultipliers in water. It detects the Cherenkov light⁽⁴⁾ produced by the secondary particles of the shower when they pass through the water. MILAGRO can detect the Crab Nebula with a significance of about 5σ in 100 days of observation, at a median energy of about 20 TeV.

⁽⁴⁾ The Cherenkov light is a radiation produced in a medium by charged particles which travel faster than the speed of light in that medium; since its differential probability is proportional to $(1/\lambda)$ in the visible, it peaks on the blue. Cherenkov photons are emitted at an angle θ_C such that $\cos(\theta_C) = \frac{1}{\beta n}$, where n is the refractive index of the medium in which the phenomenon takes place, and β is the speed of light in units of c .



Figure 22. – View of the laboratory of the ARGO detector [67].

The energy threshold of EAS detectors is at best in the 0.5 TeV-1 TeV range, and it also depends on where the first interaction of the atmospheric shower occurred, so such detectors are built to detect UHE photons as well as the most energetic VHE gammas. At such energies fluxes are small, so they need to have large surfaces, of order of 10^4 m². EAS detectors are possibly provided with a muon detector devoted to hadron rejection; otherwise the discrimination from the background can be done based on the reconstructed shower shape. The direction of the detected primary particles is computed by taking into account their arrival times, and the angular precision is about 1 degree. Energy resolution is also poor. The calibration can be performed by studying the shadow in the reconstructed directions caused by the presence of the Moon.

4'3.2. Cherenkov telescopes. Imaging Atmospheric Cherenkov Telescopes (IACTs), such as CANGAROO III, H.E.S.S., MAGIC and VERITAS, detect the Cherenkov photons produced in air by charged, locally superluminal particles in atmospheric showers. For reasons explained below, they have a low duty cycle and a small FoV, but they have



Figure 23. – The MILAGRO detector [68].

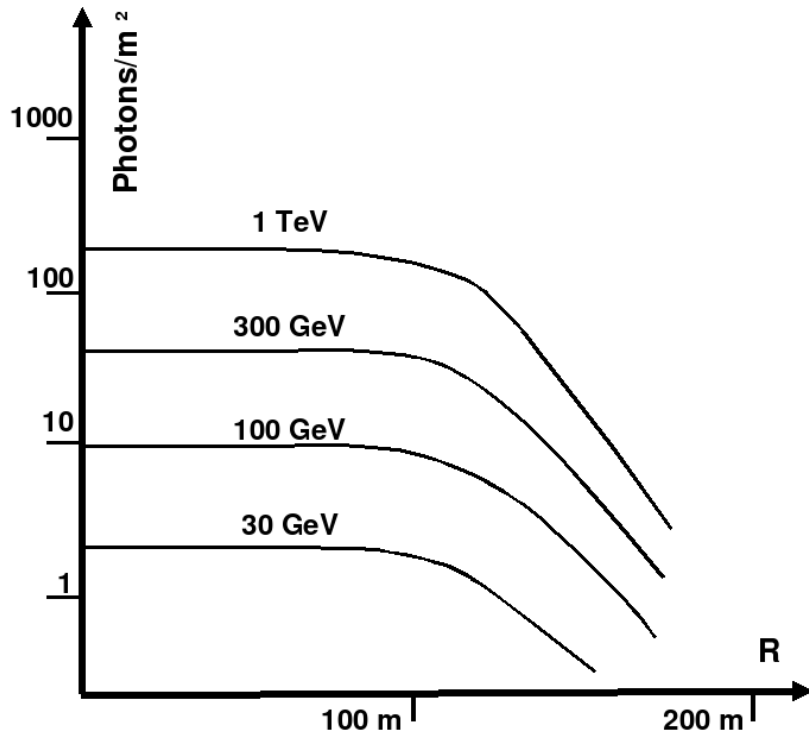


Figure 24. – Density per square meter of Cherenkov photons between 300 and 600 nm as a function of distance R from the shower impact point for various photon energies as seen at 2 km a.s.l. for vertical showers.

a high sensitivity and a low energy threshold.

At sea level, the value of the Cherenkov angle θ_C in air for $\beta = 1$ is about 1.3° , while at 8 km a.s.l. it is about 1° . The energy threshold at sea level is 21 MeV for a primary electron and 44 GeV for a primary muon.

Half of the emission occurs within 21 m of the shower axis (about 70 m for a proton shower).

Since the intrinsic angular spread of the charged particles in an electromagnetic shower is about 0.5 degrees, the opening of the light cone is dominated by the Cherenkov angle. As a consequence, the ground area illuminated by Cherenkov photons from a shower of 1 TeV (the so-called “light pool” of the shower) has a radius of about 120 m. The height of maximal emission for a primary of 1 TeV of energy is approximately 8 km a.s.l., and about 150 photons per m^2 arrive at 2000 m a.s.l. in the visible frequencies. This dependence is not linear, being the yield of about 10 photons per square meter at 100 GeV (Fig. 24). The shower has a duration of a few (about 2 to 3) ns at ground; this duration is maintained by an isochronous (parabolic) reflector.

The observational technique used by the IACTs is to project the Cherenkov light collected by a large optical reflecting surface onto a camera made by an array of photomultiplier tubes, with typical quantum efficiency of about 30%, in the focal plane of the reflector (see Fig. 25). The camera has a typical diameter of about 1 m, which corresponds to a FoV of $5^\circ \times 5^\circ$. The signal collected by the camera is analogically transmitted

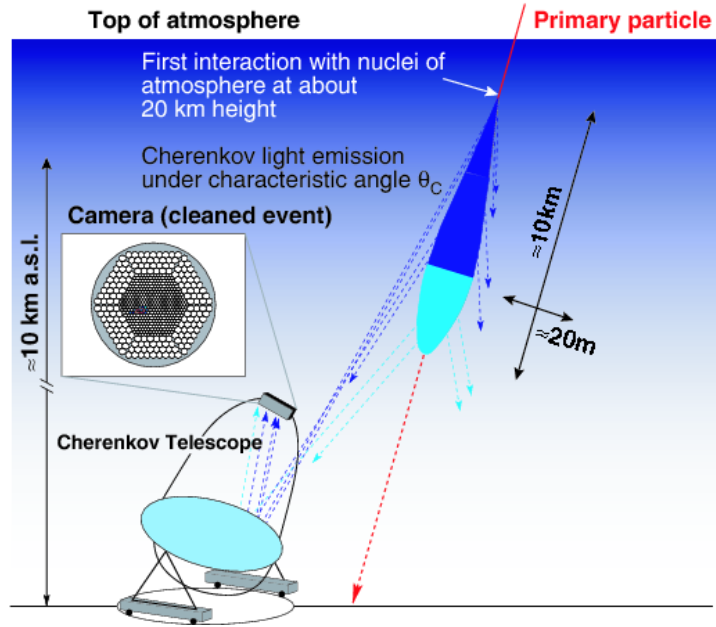


Figure 25. – The observational technique adopted by the Imaging Atmospheric Cherenkov Telescopes (IACTs) [59].

to trigger systems, similar to the ones used in high-energy physics. The events which passed the trigger levels are sent to the data acquisition system, which typically operates at a frequency of a few hundreds Hz. The typical resolution on the arrival time of a signal on a photomultiplier is better than 1 ns.

Since, as discussed above, about 10 photons per square meter arrive in the light pool for a primary photon of 100 GeV, a light collector of area 100 m² is sufficient to detect gamma-ray showers if placed at mountain-top altitudes. Due to the faintness of the signal, data can typically be taken only in moonless time, or with moderate moonlight, and without clouds, which limits the total observation time to some 1500 hours per year.

In the GeV-TeV region the background from charged particles is three orders of magnitude larger than the signal. Hadronic showers, however, have a different topology with respect to electromagnetic showers, being larger and more subject to fluctuations. One can thus separate showers induced by gamma-rays from the hadronic ones on the basis of the shower shape.

Most of the present identification techniques rely on a technique pioneered by Hillas in the 80's [69]; the discriminating variables are called “Hillas parameters”. Several new techniques have been proposed to improve these results [70]; a recent review on the problem of background subtraction is published in [71]. The intensity (and area) of the image produced is an indication of the shower energy, while the image orientation is related to the shower direction. The shape of the image is different for different primary particles, in such a way that its characteristics are used to distinguish between events produced by photons and by other particles, and to reject the background from charged particles (Fig. 26). Since the signal points to a given source, while the background is

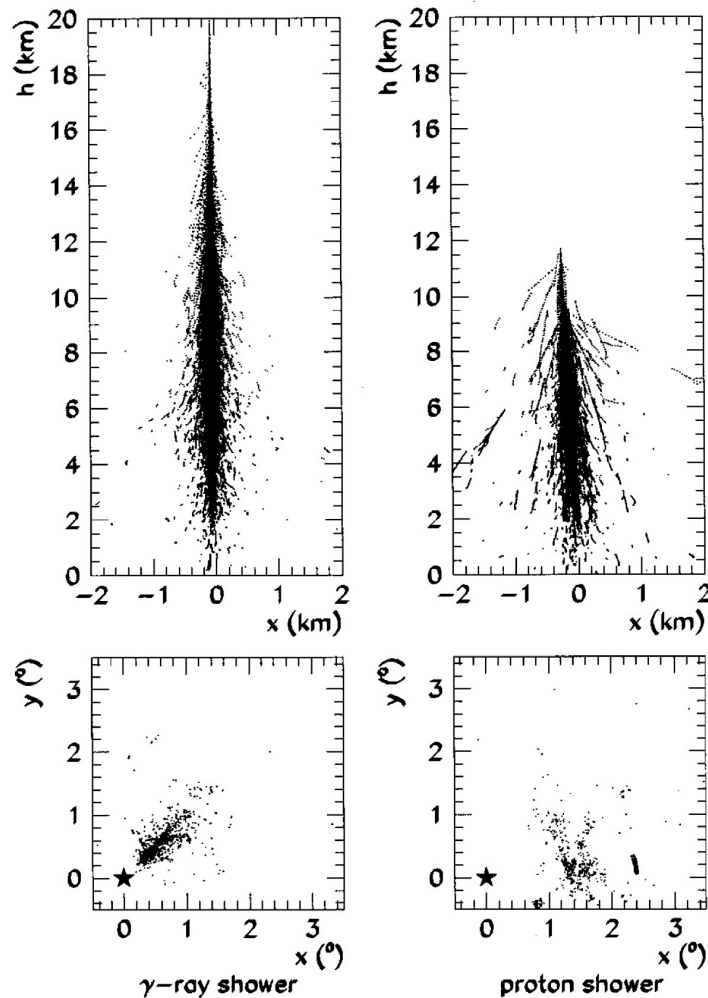


Figure 26. – Development of vertical 1-TeV proton and photon showers in the atmosphere. The upper panels show the positions in the atmosphere of all shower electrons above the Cherenkov threshold; the lower panels show the resulting Cherenkov images in the focal plane of a 10-m reflecting mirror when the showers fall 100 m from the detector (the center of the focal plane is indicated by a star) [12].

expected to be uniformly distributed, the image is circular for a shower falling directly on the detector, becoming more elliptical as the incoming photon displays a nonzero impact parameter. For a photon coming from the source, the angle α in Fig. 27 should be close to zero, while it should not peak to zero for hadrons, since their direction does not come from a single source.

The time structure of Cherenkov images provides an additional discriminator against the hadronic background [72], which can be used by isochronous detectors (with parabolic shape) and with a signal integration time smaller than the duration of the shower (i.e., better than 1-2 GHz).

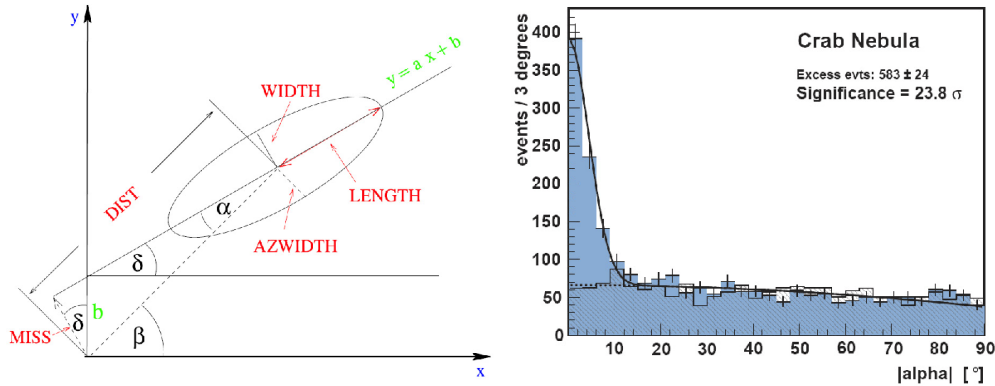


Figure 27. – Left: Imaging parameters used by air Cherenkov telescopes to reject the hadronic cosmic-ray background: α , width, and length. The ellipse represents the outline of the shower image in the focal plane of the telescope. Right: An “ α -plot” of the signal from the Crab Nebula, by the MAGIC telescope.

Two pointing modes can be used for the observation: the on-off mode and the wobble mode.

- For the on-off mode, in the “on” phase the source is located in the camera center; in a different time a similar sky region without sources is pointed, and this measurement (called “off”) is used to estimate the background. Since this cannot be done at the same time, conditions (weather, night sky background, etc.) can be different: thus an appropriate scaling of the background measurement is needed.
- Instead of observing the source in the center of the camera, the telescope can be pointed to a sky position slightly off-source. The background can then be extracted from a so called anti-source position symmetrical with respect to the camera center. This observation mode is called wobble mode. Wobble mode has in general the disadvantage of a slightly worse sensitivity, but it saves observation time.

Systems of more than one Cherenkov telescope provide a better background rejection, and a better angular and energy resolution (see Fig. 28) than a single telescope.

There are four large operating IACTs: CANGAROO III, H.E.S.S., MAGIC and VERITAS (see Fig. 29), two located in the southern hemisphere and two in the northern hemisphere.

- CANGAROO (the present setup is called CANGAROO III) is a Japanese and Australian observatory placed near Woomera (Australia). In its final design it will be a system of four telescopes with a surface of 57 m^2 each. The third telescope has been completed in 2004; its precursors, CANGAROO (single telescope) and CANGAROO II (two telescopes), started their activity in 1992 and 1999 respectively.
- The H.E.S.S. observatory (Fig. 30) is composed by four telescopes with surface of 108 m^2 each, working since early 2003, while the first of these telescopes is operating since summer 2002. It is located in the Khomas highlands of Namibia, and it involves several countries, Germany and France in particular. In the future

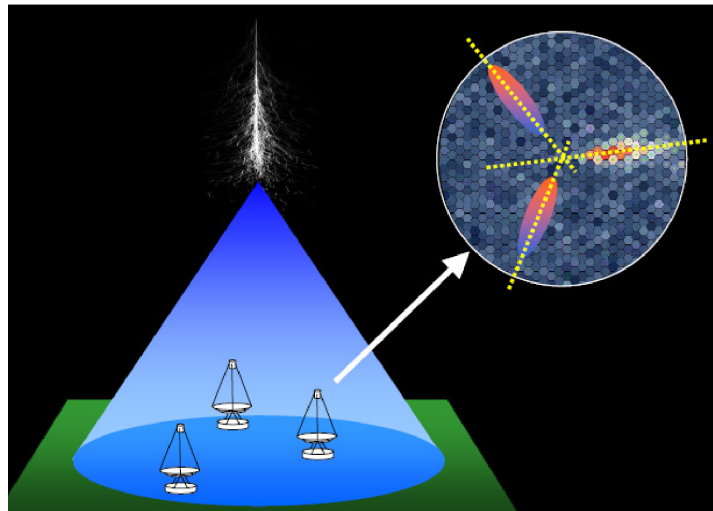


Figure 28. – A system of more than one Cherenkov telescope [73].

another telescope with a surface of about 600 m² will be placed in the center of the present array. Among the present detectors, it has the best sensitivity (about 1% Crab at 5 standard deviations in 50 hours of observation) and the best angular resolution (about 0.06 degrees, which allows imaging many galactic sources). The present energy threshold is about 100 GeV at trigger level.

- The MAGIC telescope (Fig. 31) in the Canary Island of La Palma, has a diameter of 17 m and a reflecting surface of 236 m², and it is the largest single-dish Cherenkov



Figure 29. – Location of the four big IACTs [74].



Figure 30. – The H.E.S.S. telescopes [74].

telescope in operation; due to the largest area it reaches the lowest energy threshold (about 50 GeV). The collaboration operating MAGIC involves several countries, Germany, Italy, Spain, Finland and Switzerland in particular. Besides the purpose of lowering as much as possible the energy threshold by increasing the dish size, the instrument was designed to be able to rapidly slew responding to alerts due to transient phenomena (GRBs in particular). The lightweight construction allows a slewing time of 22 s, three to four times faster than H.E.S.S. The advantages of a stereoscopic system (as discussed above) motivated the second phase of the MAGIC project: the construction of a second 17 m telescope at a distance of about 85 m from the first will increase substantially (by a factor of 2) the sensitivity of MAGIC, making it similar to the sensitivity of H.E.S.S., and improve the angular resolution from 0.1 degrees to about 0.07 degrees.



Figure 31. – The MAGIC telescope [75].



Figure 32. – The VERITAS site [76].

- VERITAS ([76]; Fig. 32) involves Canada, Ireland, the United Kingdom and the U.S.A.. The observatory is constituted by an array of four telescopes with a diameter of 12 m and is located near Tucson, Arizona. It is operative since April 2007, but the VERITAS prototype telescope was active since February 2004. The overall design is rather similar to H.E.S.S..

The main characteristics of the detectors are summarized in Table 1, adapted from Ref. [14]. Typical sensitivities of H.E.S.S., MAGIC, VERITAS are of about 1% to 2% of Crab in 50 hours of observation.

The observation at an angle different from the zenith deteriorates the energy threshold. The dependence of the threshold energy E_{thr} as a function of the angle ϕ with respect to the zenith can be parametrized as $E_{thr} \simeq E_0 \cos^{-2.5} \phi$ [77] where E_0 is the threshold for a source at the zenith. However, due to geometrical factors, the effective area increases when getting away from the zenith.

An overlap in the regions of the sky explored by the IACTs allows an almost continuous observation of sources placed at mid-latitude; there is however space for two more installations, one in South America and one (MACE, already scheduled for construction) in India.

Negotiations towards a Memorandum of Understanding is ongoing to balance compe-

TABLE I. – *Main characteristics of currently operating IACTs.*

The energy threshold given is the approximate trigger-level threshold for observations close to zenith. The approximate sensitivity is expressed as the minimum flux (as a percentage of that of the Crab Nebula: $\approx 2 \times 10^{-11}$ photons $\text{cm}^{-2} \text{s}^{-1}$ above 1 TeV) of a point-like source detectable at the 5σ significance level in a 50 hour observation.

| Instrument | Lat. (°) | Long. (°) | Alt. (m) | Tels. | Tel. Area (m ²) | Total A. (m ²) | FoV (°) | Thresh. (TeV) | Sensitivity (% Crab) |
|--------------|----------|-----------|----------|-------|-----------------------------|----------------------------|---------|---------------|----------------------|
| H.E.S.S. | -23 | 16 | 1800 | 4 | 107 | 428 | 5 | 0.1 | 0.7 |
| VERITAS | 32 | -111 | 1275 | 4 | 106 | 424 | 3.5 | 0.1 | 1 |
| MAGIC | 29 | 18 | 2225 | 1 | 236 | 236 (472)* | 3.5 | 0.05 | 1.6 (0.8) |
| CANGAROO-III | -31 | 137 | 160 | 3 | 57.3 | 172 | 4 | 0.4 | 15 |

* With MAGIC2 (September 2008).

TABLE II. – A comparison of the characteristics of GLAST, the IACTs and of the EAS particle detector arrays.

| Quantity | GLAST | IACTs | EAS |
|-------------------|------------------|----------------------|-------------------|
| Energy range | 20 MeV – 200 GeV | 100 GeV – 50 TeV | 400 GeV – 100 TeV |
| Energy resolution | 5-10% | 15-25% (*) | ~ 50% |
| Duty Cycle | 80% | 15% | > 90% |
| FoV | $4\pi/5$ | 5 deg \times 5 deg | $4\pi/6$ |
| Resolution(PSF) | 0.1 deg | 0.07 deg | 0.5 deg |
| Sensitivity(**) | 1% Crab (1 GeV) | 1% Crab (0.5 TeV) | 0.5 Crab (5 TeV) |

(*) Decreases to 15% after cross-calibration with GLAST [78].

(**) Computed over one year for GLAST and the EAS, and over 50 hours for the IACTs.

tion and cooperation among the present IACTs.

4.4. *Resumé.* – A simplified comparison of the characteristics of the GLAST LAT satellite detector, of the IACTs and of the EAS detectors (ground-based) is given in Table II. The sensitivities of the above described high-energy detectors are shown in Fig. 33.

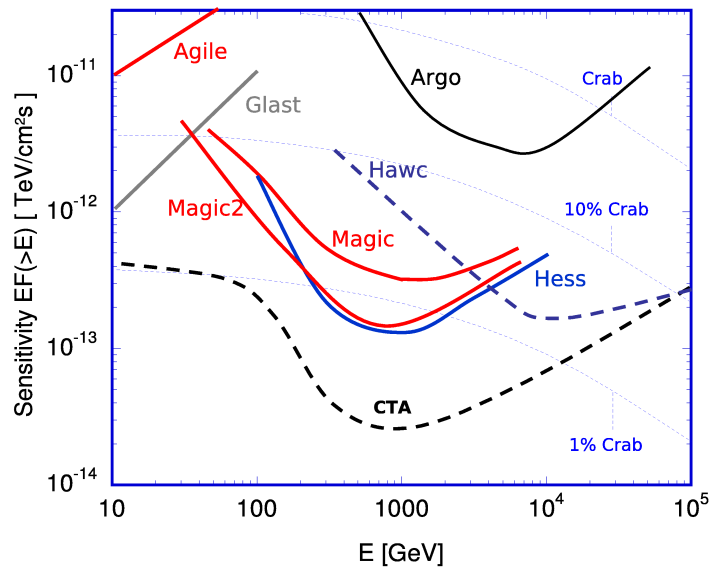


Figure 33. – Sensitivities of some present and future HE gamma detectors [79], measured as the minimum intensity source detectable at 5σ . The performance for EAS and satellite detector is based on one year of data taking; for Cherenkov telescopes it is based on 50 hours of data. The sensitivity curve for VERITAS is between MAGIC and MAGIC2.

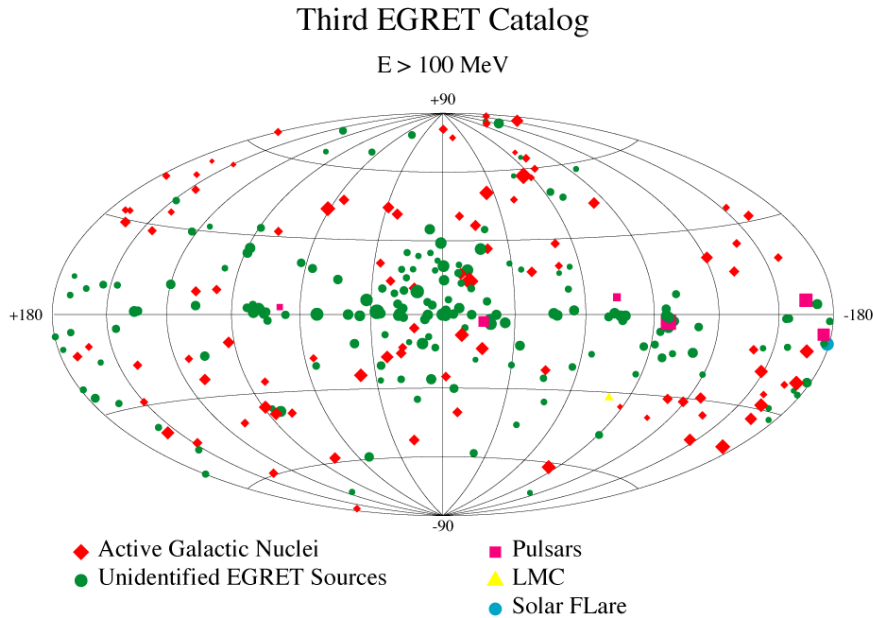


Figure 34. – Third EGRET catalog (1999) at energies greater than 100 MeV [80].

5. – The emerging HE and VHE gamma-ray sky

More than one half of the 271 sources detected at energies >100 MeV in the third EGRET catalog of 1999 (see Fig. 34) are still unidentified.

Thanks mostly to Cherenkov telescopes, a large amount of VHE sources has been detected and identified (see Fig. 35). When this review has been written (June 2008), 76 VHE sources had been detected, which operate as cosmic particle accelerators, and the γ -rays they emit trace information on the primary electrons or nuclei. Therefore, it is important to determine the nature of the primary particles and their spatial and momentum distribution. Among these sources, 8 are supernova remnants (SNRs), 14 are pulsar wind nebulae (PWNe), one is the galactic centre, 4 are binary systems, one is a VHE pulsar, 25 are unidentified galactic sources, and 23 are active galactic nuclei.

5.1. Galactic cosmic-ray accelerators. – The recent dramatic growth (by a factor of ~ 10) in the number of known galactic VHE sources is largely a consequence of the survey of the galactic plane conducted with the southern-located H.E.S.S. between 2004 and 2007 [82]. Fig. 36 shows the current extent of this scan, which now covers essentially the whole inner Galaxy: $-85^\circ < l < 60^\circ$, $-2.5^\circ < b < 2.5^\circ$ [83]. Further galactic sources, accessible from the northern hemisphere, were subsequently observed with the MAGIC telescope (e.g., Ref. [84]), and even more by H.E.S.S. Proposed counterparts of such galactic VHE sources include supernova remnants, PWNe, and accreting binaries. Whatever their detailed nature, it is expected that galactic VHE sources are related to evolutionary end-products of massive, bright, short-lived, stellar progenitors. Hence, these galactic VHE sources are immediate tracers of the current star formation.

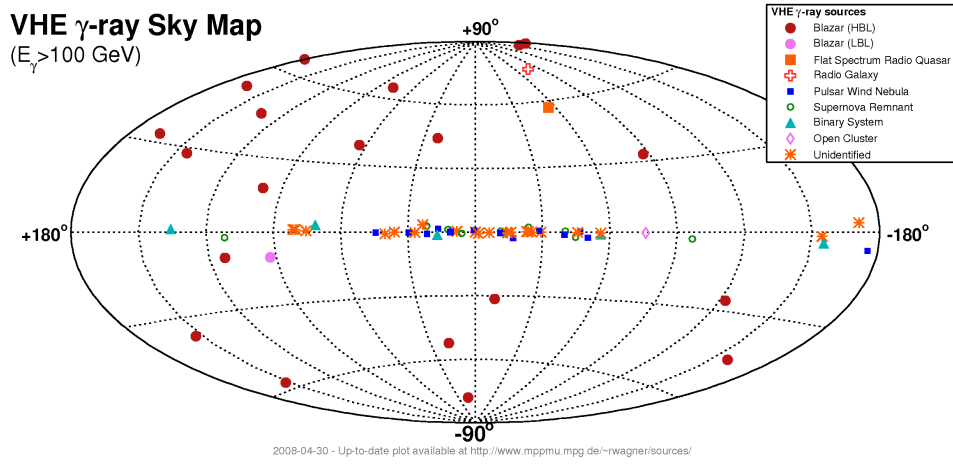


Figure 35. – Known sources in the VHE sky in 2008 [81].

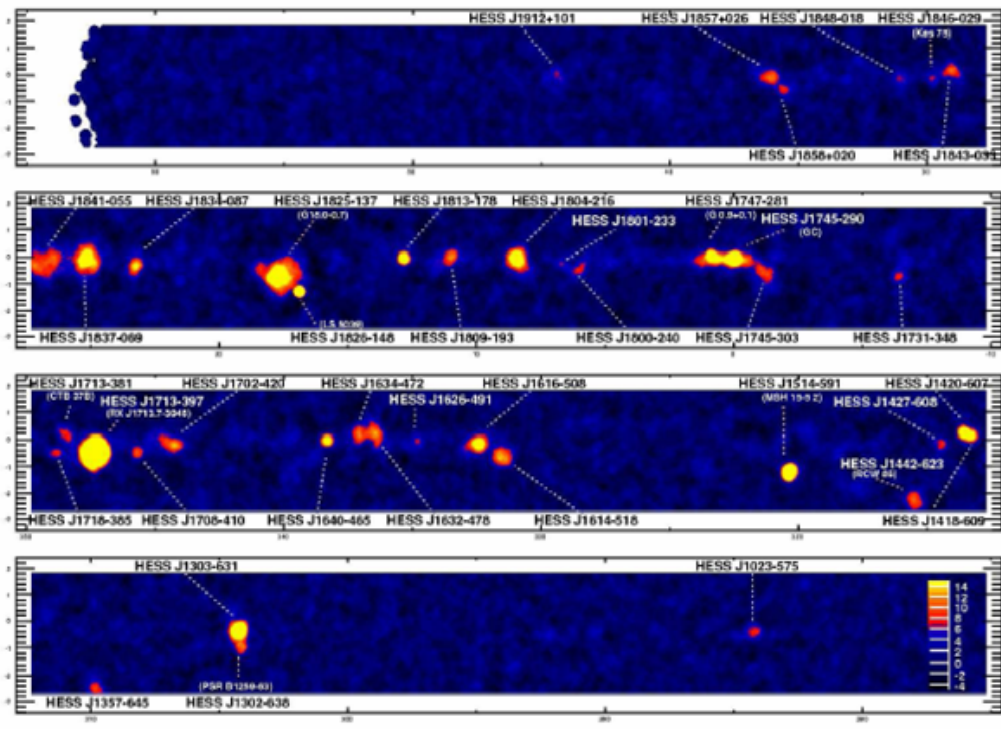


Figure 36. – Known galactic VHE sources from the survey of the galactic plane by the H.E.S.S. telescope between 2004 and 2007 [83].

About half of the currently known galactic TeV sources remain unidentified. This is in part due to the difficulty of identifying extended sources with no clear sub-structure. Nonetheless, several methods of identification have been successfully applied and the situation is much more favourable than that in the GeV band where only one galactic source class (pulsars) has been unambiguously identified.

5.1.1. Supernova Remnants. Galactic cosmic rays have long been suspected to be produced at supernova shock fronts via diffusive acceleration. If the observed VHE γ -rays were found to be generated through the hadronic channel, via π^0 decay following pp interaction with the dense molecular clouds embedding the short-lived supernova progenitor, then the acceleration by supernovae of nuclei to energies of the order of the knee in the cosmic-ray spectrum would be proven (e.g., Ref. [85]). However, it is difficult to disentangle the hadronic VHE component from the leptonic one, produced by IC scattering of interstellar radiation field photons (in the inner Galaxy) or cosmic microwave background photons (in the outer Galaxy) off ultrarelativistic electrons (e.g., Ref. [86]), by measuring γ -rays over only a decade or so in energy. The VHE data of RX J1713.7-3946 can be explained in terms of either channel, leptonic/hadronic if the relevant magnetic field is low/high ($B \sim 10/100 \mu\text{G}$ [87, 88]). Data in the ~ 0.1 –100 GeV band, such as those to be provided by AGILE and GLAST, are clearly needed to discriminate between the two channels. (For Cas A the high magnetic field, $B \sim 1$ mG, suggests a mostly hadronic [89] VHE emission [90].) The complementarity between AGILE and GLAST on one side and the IACTs on the other side might be the key for important discoveries in the future [91].

Whatever the details, the detection of photons with $E \gtrsim 100$ TeV from RX J1713.7-3946 is a proof of the acceleration of primary particles in supernova shocks to energies well above 10^{14} eV. The differential VHE spectral index is ~ 2.1 all across this SNR, suggesting that the emitting particles are ubiquitously strong-shock accelerated, up to energies $\sim 200/100$ TeV for primary cosmic protons/electrons if the hadronic/leptonic channel is at work [92]. This is getting close to the knee of the cosmic-ray spectrum; this fact might signal the high-energy end of the galactic cosmic-ray distribution (e.g. Ref. [93]).

Circumstantial evidence supports a hadronic origin for at least part of the VHE emission. In several expanding SNRs the X-ray brightness profile behind the forward shock is best explained as synchrotron emission from energetic electrons in strong magnetic fields, $B \sim \mathcal{O}(10^2) \mu\text{G}$, i.e. ~ 100 times larger than typical interstellar medium values. Such a large amplified magnetic field disfavors the IC interpretation of the VHE data. Furthermore, in the remnant HESS J1834-087, the maximum of the extended VHE emission correlates with a maximum in the density of a nearby molecular cloud [94] – which suggests hadronic illumination of the target molecular cloud. A similar situation holds for IC 443 [95] and W 28 [96], both of which appear to have emission correlated with available target material rather than with the radio/X-ray emission of the SNR itself, suggesting that the VHE emission may arise from hadronic interactions in/around the SNR.

5.1.2. Pulsars and Pulsar Wind Nebulae. Pulsars are understood as rapidly spinning neutron stars (with periods between about 1 ms and 1 s) with extremely strong magnetic fields. (Neutron stars are stellar remnants of supernova explosions.) Pacini [97] argued that such stellar remnants could power SNRs like the Crab nebula, and predicted that they could be observable at radio frequencies. Rotation generates an induced electric field

that overcomes gravity, so charges are pulled out from the neutron star surface (where a layer of plasma still survives), in the form of a relativistic wind that carries most of the pulsar’s rotational energy, filling the (corotating) magnetosphere with plasma. Electron-positron pairs originate in the magnetosphere via interaction with the magnetic field; they may escape through the polar cap regions in the form of a wind that eventually terminates in the surrounding interstellar medium.

Gamma-ray radiation from rotation-powered pulsars can be produced through several radiation mechanisms in three physically distinct regions: magnetosphere, relativistic wind, and the surrounding nebula. As for the latter, the pair-wind termination shock into the circumstellar medium establishes a standing reverse shock: this leads to the formation of a nonthermal (synchrotron and Compton) nebula whose spectrum extends from radio to VHE gammarays.

To date there is no wide consensus on the physical mechanism for magnetospheric emission. Objects emitting at X-ray to γ -ray energies are critical to this scope, because this energy band is where most of the radiative luminosity is observed and it is linked with the pair wind that is the dominant mode of energy deposition in the circum-pulsar environment. The most crucial issue about this high-energy emission of pulsars is the location of the acceleration region in the magnetosphere: is it in the outer gap (e.g., Ref. [98, 99]; review by [100]) or in the polar cap (e.g., Ref. [101]; review by [102]). Different radiative signatures are predicted in the two cases.

The key difference between the two models is the location of the acceleration zone: near the pulsar surface, i.e. at the magnetic poles (polar-cap model), or further out from the star surface, where the local field is reduced by several orders of magnitudes with respect to the field at the star’s surface (outer-gap model). In terms of observables, this distinction translates into the manifestation (or lack thereof) of extremely strong magnetic fields.

In polar-cap models, for strong values of the magnetic field ($10^{11}\text{G} \lesssim B \lesssim 4 \times 10^{13}\text{G}$), the conversion of photons into e^+e^- pairs generates cascades that strongly attenuate supra-GeV emission in Crab-like or Vela-like (“canonical”) pulsars, generating steeper-than-exponential (“super-exponential”) cutoffs in the 10 MeV – 10 GeV band⁽⁵⁾. In outer-gap models pair creation is obtained through the $\gamma\gamma \rightarrow e^+e^-$ process involving surface thermal X-rays as targets, and the absorption of γ -rays in the magnetic field is not sufficient for the development of pair cascades and does not significantly distort the emitted spectrum.

Discrimination between different polar-cap versus outer-gap models of pulsar magnetospheric emission is one clear goal of VHE astrophysics.

The current observational situation is exemplified by the cases of the PSR B1951+32 and Vela pulsars [103, 104]. In the latter case upper limits to the pulsed emission imply a cutoff energy $E_c < 32$ GeV. In both, Vela and PSR B1951+32, IC emission at TeV energies as predicted by outer-gap models is severely constrained, although not all outer-gap models are ruled out. Deeper sensitivities can test the models further, and certainly no test of these models in the range 10–100 GeV has yet been achieved.

Millisecond pulsars, that have lower magnetic fields, in polar-cap models could have a cutoff at ~ 100 GeV (i.e., $E_c \propto B^{-1}$), hence their (pulsed) VHE emission could be relevant. Detecting it would be a test of the polar-cap theory [105].

⁽⁵⁾ For magnetars, pulsars with still higher fields, $B > 4 \times 10^{13}\text{G}$, no emission is predicted above >100 MeV.

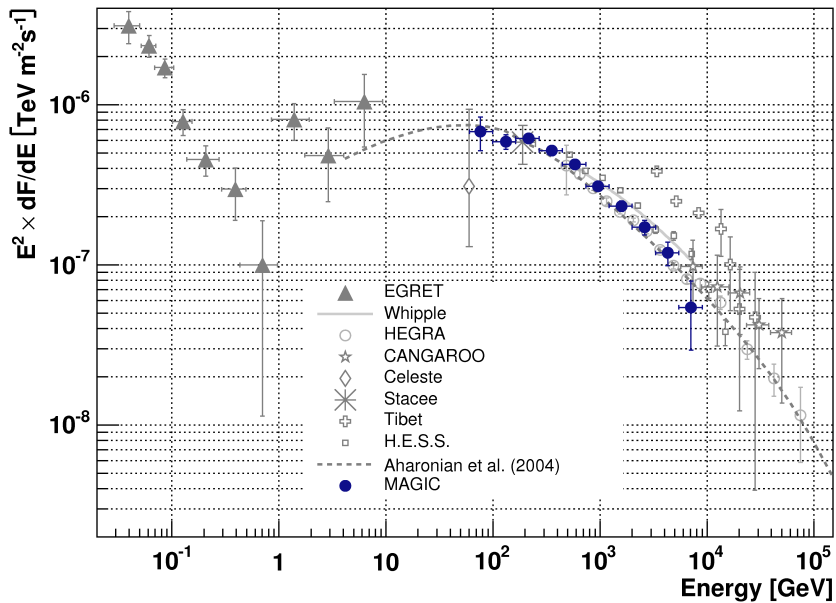


Figure 37. – The spectrum of the Crab Nebula in the HE region [106].

The Crab Nebula was the first VHE source to be discovered [15]. It still is the brightest steady emitter in the VHE sky, that is used as a calibration candle. The γ -ray emission from the Crab is dominated by the pulsed emission from the rotating pulsar below GeV energies, and by the steady emission from the nebula above GeV energies. Its broad-band spectrum is double-peaked (see Fig. 37), a feature common to all pulsar wind nebulae: the two components are usually attributed to synchrotron radiation and its Compton scattering off the parent relativistic electrons that emerge from the termination shock of the pulsar wind. Its spectral energy density decreases in the GeV region, but it has a turn-over and starts to be again visible at about 100 GeV. The Crab Nebula has been observed extensively from the radio energy range up to about 70 TeV. No pulsed (magnetospheric) VHE emission was originally found in MAGIC data from previous observational campaigns, that implies $E_c < 50$ GeV [106]. The steady nebular spectrum, measured in the about 0.03-30 GeV range by EGRET and in the about 0.06-70 TeV by several IACTs, shows a bump that starts to dominate at about 1 GeV and peaks at about 50 GeV: this component results from IC scattering, by the synchrotron-emitting electrons, of softer photons in the shocked wind region – i.e., synchrotron, far infrared/millimeter or cosmic microwave background photons. In spite of its detected IC γ -ray emission, however, the Crab Nebula is not an effective IC emitter as a consequence of its high nebular magnetic field ($B \sim 0.4$ mG).

Very recently, the MAGIC collaboration has reported on the detection of the Crab pulsar [107]. The source was observed from October 2007 until February 2008 for 40 hours, of which 22 hours of data were recorded at optimal weather condition and small zenith angles. The observation took place after the installation of a new trigger system which lowered the threshold from 50-60 GeV down to 25 GeV. The analysis reveals a

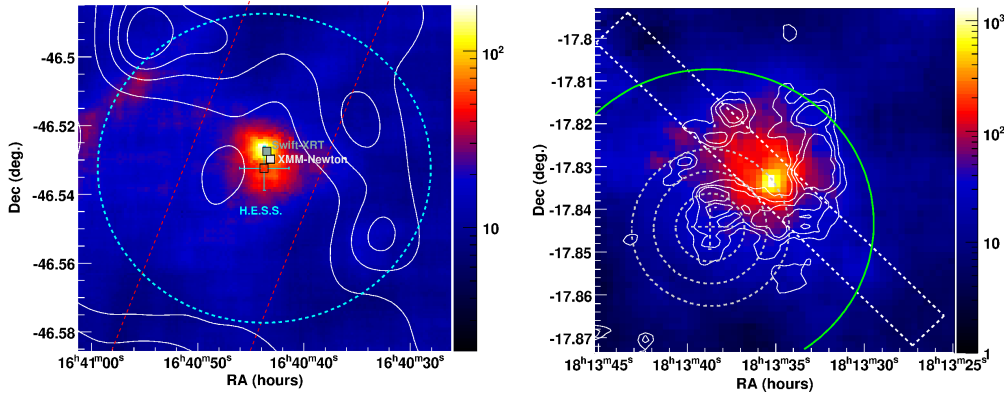


Figure 38. – Sky map around HESS J1640-465 [109] (left) and around HESS J1813.178 [110] (right).

pulse profile that shows a very clear signal at a 6.4σ level coinciding also with an optical signal concurrently recorded by a special photosensor in the camera center. Both peaks in the light curve, the main pulse and the interpulse, are of about equal intensity. Both are clearly visible and are in phase with the emission at all other lower energies including gamma energies above 100 MeV as observed by EGRET.

The γ -ray energy cutoff will be deduced for the first time, allowing a direct comparison with emission models [107].

Pulsar wind nebulae – PWNe are pulsars displaying a prominent nebular emission. They currently constitute the most populated class of identified galactic VHE sources (7 identifications – see e.g. Ref. [108]). Even for the unidentified extended VHE sources detected in the H.E.S.S. galactic plane survey, there is a clear excess of VHE nebulae positionally coincident with high-luminosity radio pulsars. So probably the class of PWN is even more populated than it appears now. Some PWNe have an X-ray counterpart: HESS J1640-465 [109] and HESS J1813.178 [110] (see Fig. 38); the second source has a radio shell [111].

Also based on the observed X-ray emission, we can assume that the VHE emission of PWNe is likely of leptonic origin. Let us consider the case of HESS J1825-137, for which spectra have been measured in spatially separated regions [112]. In these regions, the VHE spectra become steeper with increasing distance from the pulsar, and the VHE morphology is similar to the X-ray morphology: furthermore the low derived magnetic field (few μG) implies that synchrotron X-ray emission is due to electrons of energy higher than the γ -rays. This suggests that the observations can be modeled in terms of very energetic electrons that efficiently lose energy via synchrotron losses, aging progressively more rapidly as they are farther away from the acceleration site, and produce VHE γ -rays via IC scattering.

The PWNe seen by H.E.S.S. are extended sources with dimension of order of 10 pc, in several cases displaced with respect to the pulsar they contain. This may be due to the supernova explosion occurring in an inhomogeneous medium, and the resulting asymmetric reverse shock displacing the PWN in the direction away from the higher-density medium. Such an offset may be typical of older PWNe, e.g. Vela (spin-down age: 11kyr) versus Crab (1.2 kyr) (e.g., [108]).

5.1.3. Binary systems. In both SNRs and PWNe particle acceleration proceeds on the parsec distance scales in the shocks formed in interactions of either the ejecta of supernovae or pulsar winds with the interstellar medium. A different population of much more compact particle accelerators, which has been revealed by current IACTs, is formed by the TeV binaries. These systems contain a compact object – either a neutron star or a black hole – that accretes, or interacts with, matter outflowing from a companion star: hence they are VHE-loud X-ray binaries. Four TeV binaries have been detected so far: PSR B1259-63 [113], LS 5039 [114, 115], LSI+61 303 [116], and Cyg X-1 [117].

PSR B1259-63 is powered by the rotation energy of its young 48 ms pulsar, and strong VHE emission is observed from this system in pre- and post-periastron phases when the relativistic pulsar wind collides with the dense equatorial wind blowing from the companion star, which displays a rapid rotation.

LSI+61 303 and LS 5039 may share a similar structure. The former is composed of a compact object and a rapidly rotating star in a highly eccentric orbit. Its VHE emission, whose variability constrains the emitting region of LSI+61 303 to be larger than the size of the binary system, appears correlated with the radio emission and does not peak at periastron, where the rate \dot{M} of the transferred mass is expected to be largest. This picture favors an IC origin of VHE emission, as probably the most efficient at the relatively large scales of the system at peak emission. LS 5039 clearly shows periodicity of 3.9 days from the gamma-ray data alone (in agreement with the optical): the VHE spectrum varies as a function of phase, getting softer when the compact object is hidden by the companion, that may indicate photon-photon absorption or cascading.

The emission from Cyg X-1 (for which there is evidence with a significance $\gtrsim 4\sigma$) is point-like and excludes the nearby radio nebula powered by the relativistic jet. If confirmed, Cyg X-1 is the first stellar-mass ($\sim 13 M_{\odot}$) black hole, and hence the first established accreting binary, established as a VHE source.

5.1.4. The centre of the Milky Way. The possibility of indirect dark matter detection through its annihilation into VHE γ -rays has aroused interest to observe the centre of the Milky Way. H.E.S.S. and MAGIC observed the galactic centre, measuring a steady flux consistent with a differential power-law with a spectral index of about 2.2 (see Fig. 39), up to energies of about 20 TeV with no apparent cutoff [118, 119]. The γ -ray source is steady even during X-ray flares and behaves like a point source. Within the error circle of the measurement of the central source HESS J1745-290 (the position of the centre of the Milky Way is determined within a systematic error of $6''$ and a statistical error of $6''$, too) there are three compelling candidates for the origin of the VHE emission: the shell-type SNR Sgr A East, the newly discovered PWN G 359.95-0.04, and the supermassive black hole Sgr A* itself. Plausible radiation mechanisms include IC scattering of energetic electrons, the decay of pions produced in the interactions of energetic hadrons with the interstellar medium or dense radiation fields, and curvature radiation of UHE protons close to Sgr A*. These considerations disfavor dark matter annihilation as the main origin of the detected flux, whereas a more conventional astrophysical mechanism is likely to be at work (e.g., Ref. [120]). Furthermore, the lack of flux variability on hour/day/year timescales might suggest that particle acceleration occurs in a steady object, such as a SNR or a PWN, and not in the central black hole.

The diffuse emission correlates with molecular clouds and suggests an enhanced cosmic-ray spectrum in the galactic centre [36]. Its morphology and spectrum suggest recent in situ cosmic-ray acceleration: because the photon indexes of the diffuse emission and of the central source HESS J1745-290 are similar, the latter source could be the

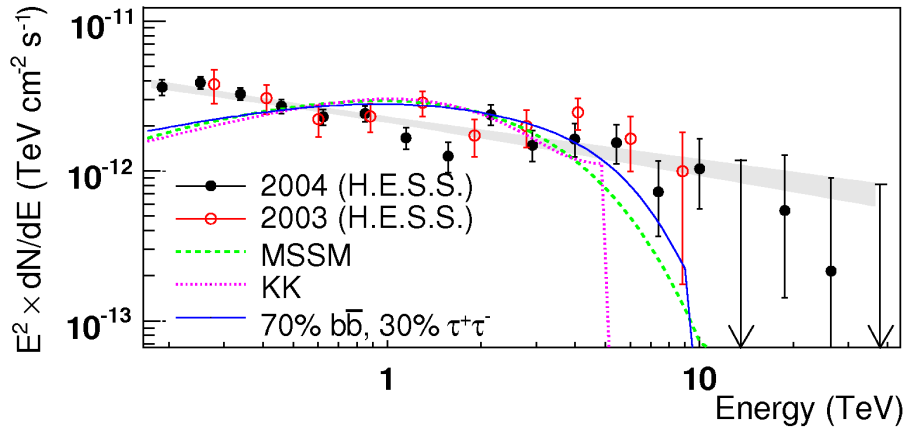


Figure 39. – Differential gamma spectrum from the galactic centre [120].

accelerator in question.

5.1.5. Mystery sources and Cygnus region. There are examples of galactic VHE sources which do not have a counterpart in the X or radio energy bands (see Fig. 40). This situation is the likely outcome of experimental and physical considerations. As an example of the former, extended sources may have different morphologies at different frequencies; as for the latter, sources may emit substantially in the GeV-TeV range and negligibly in other spectral bands (“dark accelerators”), e.g. TeV J2023+4130. Whatever their detailed nature, a reasonable expectation is that these sources, too, are related to compact stellar endproducts and descend from massive, bright, short-lived, progenitor stars. Hence, these dark accelerators would still be linked to current star-formation activity.

MAGIC, HEGRA and Whipple observed the source TeV J2023+4130 (see Fig. 41). Whipple detected it at 6.1σ with a flux corresponding to 8% of the Crab flux [122]; MAGIC observed it at 6σ with a flux 4% of the Crab flux, a size of $6'$ and a spectral index of 1.8 [123], while HEGRA detected it at 7σ with a flux 5% of the Crab flux, a size of $6'$ and a spectral index of 1.9 [124].

The MILAGRO telescope discovered the three sources MGRO J2031+41, MGRO J2019+37, and MGRO J1908+06 [125] (see Fig. 42). The second source was also seen by the EAS detector TIBET AS- γ [126]. The source MGRO J1908+06 is still unidentified; the H.E.S.S. observations in its direction are shown in Fig. 43.

Explanations for these unidentified sources range from exotic to conventional. One of the former type is that these sources originate from the annihilation of dark matter in localised clumps, i.e. subhalos within the Galaxy’s halo. A more conventional explanation is that they originate from the collision of cosmic hadrons (pp interaction), which entails emission mostly in the VHE band - contrary to electrons which typically produce comparable fluxes by synchrotron emission. However, even in this conventional scenario, the acceleration site for these hadrons remains unknown (see [128, 129]).

5.2. Extragalactic sources of VHE γ -rays. –

5.2.1. Satellites of the Milky Way. Outlooks for WIMP annihilation detection in Draco by current IACTs are not very promising: for a neutralino mass $m_\chi=100$ GeV and a

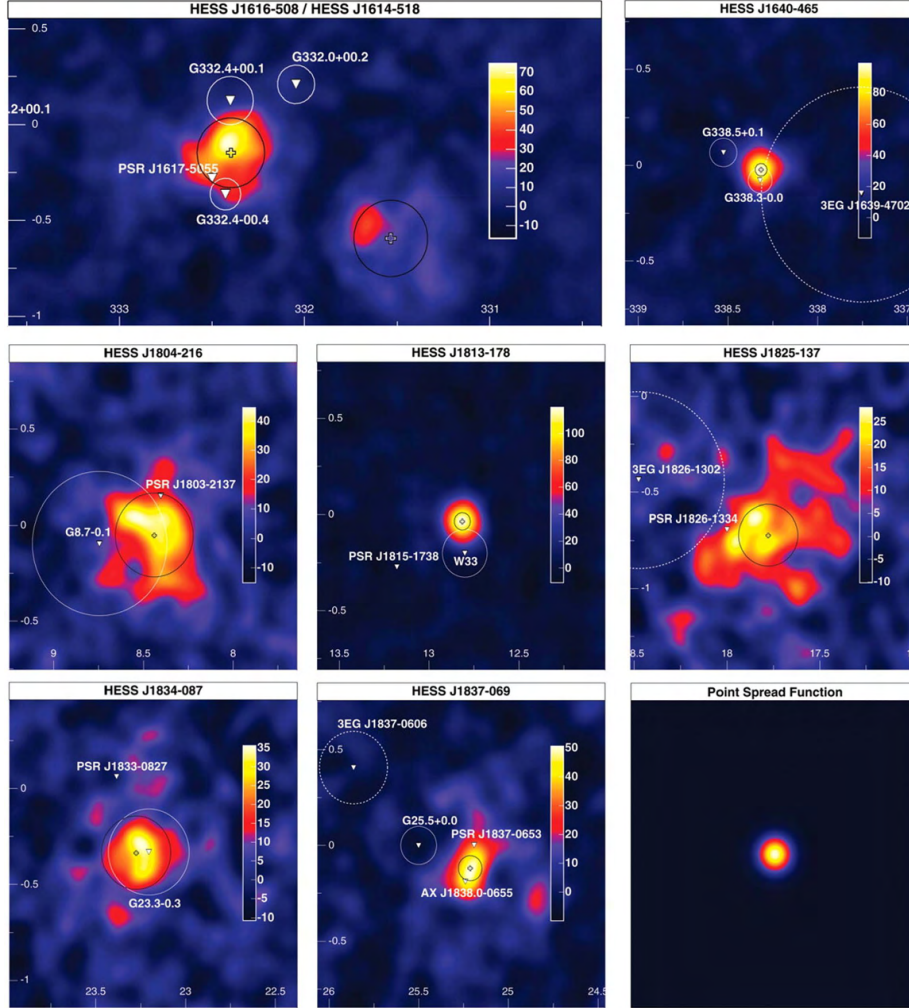


Figure 40. – Some H.E.S.S. sources without a X or radio counterpart [121].

variety of annihilation modes, and in the favorable case of a maximal (cuspy) inner halo profile, VHE detection can occur with 40h by a IACT if the average value of the neutralino cross section times the velocity is $\langle\sigma v\rangle \gtrsim 10^{-25} \text{ cm}^3\text{s}^{-1}$, which is somewhat larger than the maximum value for a thermal relic with a density equal to the measured (cold) dark matter density. The prospects are better in the HE range with GLAST (100 MeV–10 GeV): for a maximal (cuspy) halo, 1 yr of GLAST observation should be able to yield a detection if $m_\chi \lesssim 500 \text{ GeV}$ and $\langle\sigma v\rangle \sim 3 \times 10^{-25} \text{ cm}^3\text{s}^{-1}$ [130].

No evidence of dark matter annihilation γ -rays has been unambiguously claimed so far [131]. An apparently extended signal from the direction of NGC 253 has been definitely interpreted as due to hardware malfunction [132].

5.2.2. Star-forming galaxies. Diffuse γ -ray emission from pp interactions of cosmic-ray nuclei with target interstellar medium photons makes up about 90% of the $> 100 \text{ MeV}$

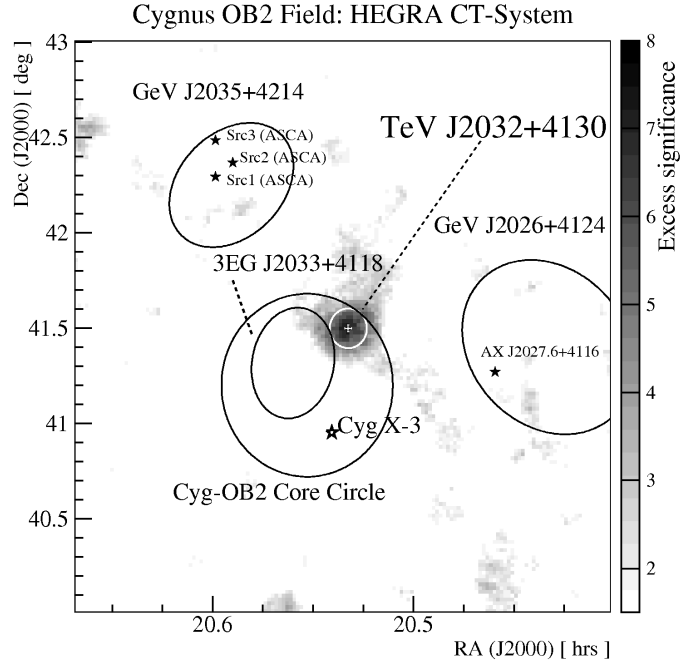


Figure 41. – The source TeV J2023+4130 as seen by HEGRA [124].

luminosity of the Milky Way [133]. However, the VHE flux from a galaxy like the Milky Way located 1 Mpc away would be well below current IACT sensitivities. Indeed, only loose upper limits on the VHE flux from normal galaxies have been obtained, even for local galaxies and for the VHE-bright starburst galaxies (e.g., Ref. [134]). Detailed models of VHE emission from NGC 253 [135, 136, 137] and for Arp 220 [134] are only weakly constrained by current upper limits [138, 139]. The increasingly deep upper limit, even for the more prominent star-forming galaxies, suggest that non-beamed emission from extragalactic distances may be beyond detection for current IACTs and possibly within reach for upcoming and future instruments [141].

5.2.3. Active Galactic Nuclei. Synchrotron-Compton models have long provided the mainstream theoretical framework to model AGN emission [25]. VHE data have been crucial to close the model, initially introduced to explain the radio-to-X-ray data that were interpreted as synchrotron radiation. For example, let us consider the simplest scheme of blazar emission, where one blob of magnetized nonthermal plasma, moving relativistically towards the observer, emits via synchrotron and Compton mechanisms (the latter, scattering synchrotron off their parent electrons). The observed synchrotron emission shows a degeneracy between the value of the magnetic field and the electron number density; the Compton emission provides the second condition needed to break the degeneracy. In general, knowledge of the whole spectral energy distribution is required for a complete description of the emitting electrons' distribution and environment (e.g., Ref. [140]). As is clear from basic knowledge of the synchrotron and Compton radiation

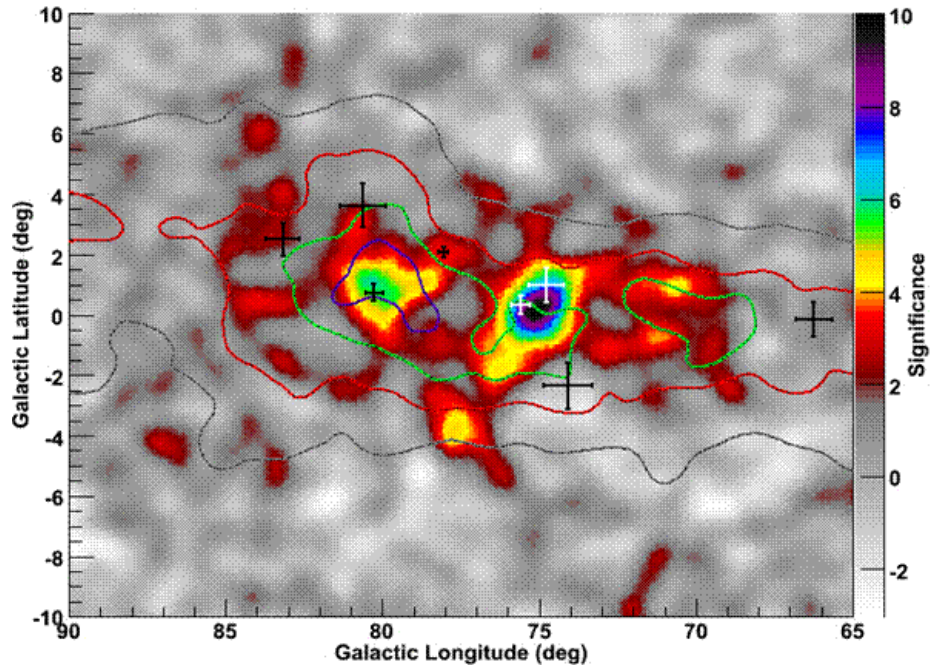


Figure 42. – The sources MGRO J2031+41 and MGRO J2019+37 as seen by MILAGRO (picture from the first paper cited in Ref. [125]).

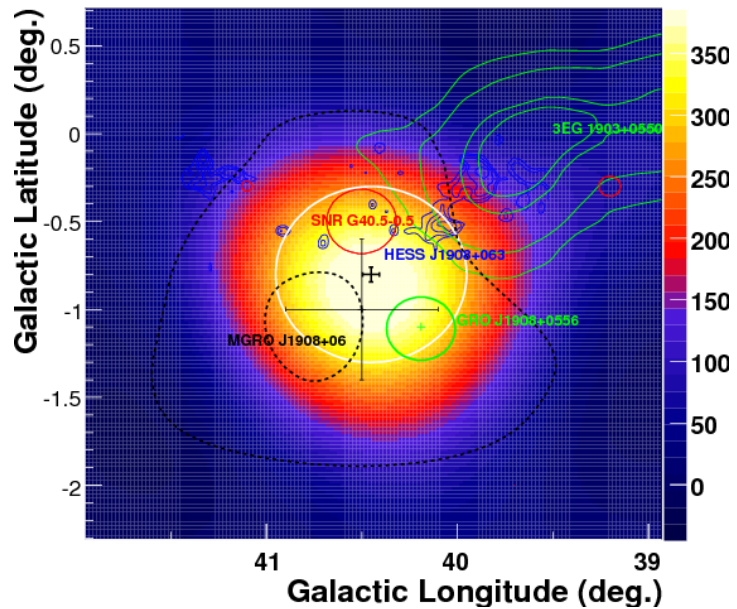


Figure 43. – The source MGRO J1908+06 [127].

mechanism, the parameters that specify the properties of the emitting plasma in the SSC model are the electron spectrum, the magnetic field, and the size and Lorentz factor of the plasma itself. Truly, a simultaneous spectral energy distribution provides us with a snapshot of the emitting population of particles at a given time.

The VHE emission of blazars has also been interpreted as due to accelerated hadrons. This possibility is particularly exciting in view of the recently claimed association of the arrival directions ultra-high-energy cosmic rays with the sky position of nearby AGNs [8].

At high energy, the 3rd EGRET catalogue [142] includes more than 130 sources known to be extragalactic (e.g., Ref. [19]), all of which are AGN (except the Large Magellanic Cloud), and about 97% of which are blazars. Of these, about 93% are low-frequency-peaked blazars (LBLs) and only about 3% are high-frequency-peaked blazars (HBLs). Therefore, blazars – mostly of the LBL type – dominate EGRET’s extragalactic HE sky. Blazars dominate the extragalactic VHE sky, too. However, these are mostly HBLs – at present, only 1/16 is of the LBL type. The HBL dominance descends from a selection bias: for a given HE flux, HBLs have a higher VHE flux than LBLs, because both spectral humps are shifted to higher frequencies.

Blazar observations have been a top priority for VHE astrophysics ever since the discovery of TeV emission from Mrk 421 [143]. To date, firm VHE detections of AGN include about 20 blazars (see Ref. [144]), the quasar 3C 279, and the radio galaxy M 87 (Ref. [150]).

After concluding that the extragalactic HE γ -ray sky is dominated by blazars, one comment is in order. Given their peculiar orientation, blazars are rare. Assuming that the maximum angle with respect to the line of sight an AGN jet can have for a source to be called a blazar is about 15° , only about 3% of all radio-loud AGN, and therefore about 0.3% of all AGN, are blazars. Assuming that about 1% of the galaxies host an AGN, this implies that only 1 out of about 30 000 galaxies is a blazar. Hence, the fact that the GeV and TeV skies are dominated by blazars is surprising. The explanation stems of course from the blazars’ defining characteristics:

- *high-energy electrons*: in some blazars the synchrotron emission peaks in the X-ray range: this suggests the presence of high-energy electrons that can produce HE/VHE radiation via Compton scattering;
- *strong non-thermal (jet) component*: HE/VHE emission is clearly non-thermal and related to the jet: the stronger the latter, the stronger the former; and
- *relativistic beaming*: in sources as compact as blazars (as suggested by their short variability timescales) all GeV photons, would be absorbed through pair-producing $\gamma\gamma$ collisions with target X-ray photons.

Beaming ensures the intrinsic radiation density to be much smaller than the observed one, so that VHE photons encounter a much lower $\gamma\gamma$ opacity and hence manage to leave the source. Furthermore, relativistic beaming causes a strong amplification of the jet’s observed flux, so providing a powerful bias toward blazar detection.

The known TeV blazars are variable in flux in all wavebands. Even simple one-zone homogeneous SSC modeling predicts the X-ray and TeV flux variability to be closely correlated, both emissions being linked to the same electron population. Observational evidence, although still statistically limited, supports this prediction (e.g., Ref. [145]). Blazar variability, both in flux and spectrum, has been observed at VHE frequencies down to minute timescales. For Mkn 501, observed with the MAGIC telescope at > 100 GeV

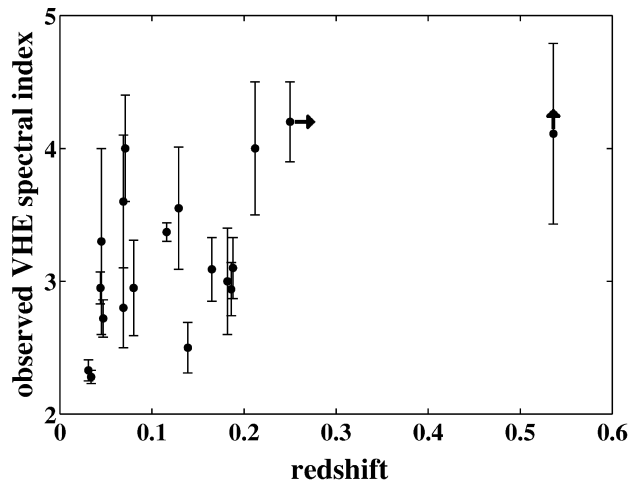


Figure 44. – Observed spectral indexes for AGN in the VHE region.

during 24 nights between May and July 2005, the integrated flux and the differential photon spectra could be measured on a night-by-night basis [146]. During the observational campaign, the flux variations (from about 0.4 to about 4 Crab units) were correlated with the spectral changes (i.e., harder spectra for higher fluxes), and a spectral peak showed up during the most active phases. A rapid flare occurred on the night of July 10th, 2005, showing a doubling time as short as about 2 minutes and a delay of about 3 minutes as a function of energy of the emitted photons.

One further aspect of TeV spectra of blazars is that they can be used as probes of the EBL. The TeV photons emitted by a blazar interact with the EBL photons and are likely absorbed via pair production. Whatever its intrinsic shape at emission, after traveling through the EBL-filled space, a blazar spectrum will reach the observer distorted by absorption. The strength of the absorption is measured by the optical depth $\tau(E, z)$ for the attenuation between the blazar, located at a distance redshift z , and the Earth [147, 42]. Usually, either (i) the shape and intensity of $EBL(z)$ is assumed, and the TeV spectrum is corrected before the SSC modeling is performed (e.g., Ref. [148, 53]); or (ii) based on assumptions on the intrinsic VHE spectrum, $EBL(z)$ is solved for: e.g., based on analysis of the observed hard VHE spectra of the distant blazars 1ES 1101-232 and H 2359-309, a low EBL energy density at $z \lesssim 0.2$ has been derived [43]. The two approaches can be used in combination to estimate the distance to the VHE source [149]. Based on the inferred attenuation of blazar VHE emission by the EBL, and in particular on the detection of the distant ($z=0.536$) quasar 3C 279 (see below), the transparency of the Universe at VHE γ -rays is deduced to be maximal, at the level implied by the known cosmic evolution of the stellar populations of galaxies.

More than 20 AGN have been detected as VHE sources (see Table III) by the time this review is written (May 2008). The AGN observed at VHE are uniformly distributed in the high galactic latitude sky. Measured spectral indices are plotted versus redshift in Fig. 44.

Currently, the most distant established VHE source is 3C 279, with $z = 0.536$. This AGN is a Flat Spectrum Radio Quasar (FSRQ) that was observed by EGRET to be

TABLE III. – *Detected AGN at TeV energies [144].*

| Source | z | α_γ | F_γ | IACT | References |
|---------------|---------|-----------------|----------------------------------|------|-----------------|
| M 87 | 0.0044 | | | H | [150] |
| Mrk 421 | 0.031 | 2.33 ± 0.08 | $1.03(\pm 0.03) \times 10^{-10}$ | M | [151] |
| Mrk 501 | 0.034 | 2.28 ± 0.05 | $1.71(\pm 0.11) \times 10^{-11}$ | M | [146] |
| | | 2.45 ± 0.07 | $3.84(\pm 1.00) \times 10^{-12}$ | M | |
| 1ES 2344+514 | 0.044 | 2.95 ± 0.12 | $1.21(\pm 0.10) \times 10^{-11}$ | M | [152] |
| Mrk 180 | 0.045 | 3.30 ± 0.70 | $8.46(\pm 3.38) \times 10^{-12}$ | M | [153] |
| 1ES 1959+650 | 0.047 | 2.72 ± 0.14 | $3.04(\pm 0.35) \times 10^{-11}$ | M | [154] |
| BL Lacertae | 0.069 | 3.60 ± 0.50 | $3.28(\pm 0.26) \times 10^{-12}$ | M | [155] |
| PKS 0548-322 | 0.069 | 2.80 ± 0.30 | $3.3(\pm 0.7) \times 10^{-12}$ | H | [156] |
| PKS 2005-489 | 0.071 | 4.00 ± 0.40 | $3.32(\pm 0.48) \times 10^{-12}$ | H | [157, 158] |
| RGB J0152+017 | 0.080 | 2.95 ± 0.36 | $4.43(\pm 1.24) \times 10^{-12}$ | H | [159, 160] |
| W Comae | 0.102 | | | V | [161] |
| PKS 2155-304 | 0.116 | 3.37 ± 0.07 | $2.89(\pm 0.18) \times 10^{-11}$ | H | [162] |
| 1ES 1426+428 | 0.129 | 3.55 ± 0.46 | $2.53(\pm 0.43) \times 10^{-11}$ | W | [163, 164] |
| 1ES 0806+524 | 0.138 | | | V | [165] |
| 1ES 0229+200 | 0.139 | 2.50 ± 0.19 | $4.46(\pm 0.71) \times 10^{-12}$ | H | [166, 167, 168] |
| H 2356-309 | 0.165 | 3.09 ± 0.24 | $2.55(\pm 0.68) \times 10^{-12}$ | H | [169, 170] |
| 1ES 1218+304 | 0.182 | 3.00 ± 0.40 | $1.01(\pm 0.26) \times 10^{-11}$ | M | [171] |
| 1ES 1101-232 | 0.186 | 2.94 ± 0.20 | $4.35(\pm 0.69) \times 10^{-12}$ | H | [172] |
| 1ES 0347-121 | 0.188 | 3.10 ± 0.23 | $3.86(\pm 0.73) \times 10^{-12}$ | H | [173] |
| 1ES 1011+496 | 0.212 | 4.00 ± 0.50 | $6.40(\pm 0.32) \times 10^{-12}$ | M | [174] |
| PG 1553+113 | >0.25 | 4.20 ± 0.30 | $5.24(\pm 0.87) \times 10^{-12}$ | M,H | [175] |
| 3C 279 | 0.536 | 4.1 ± 0.7 | $2.9(\pm 0.5) \times 10^{-11}$ | M | [176] |
| S5 0716+714 | | | $\sim \times 10^{-11}$ | M | [177] |

The observed photon spectral index α_γ between 0.2 TeV and 2 TeV (0.6 TeV for 3C279: the absolute value of the spectral index between 0.2 TeV and 2 TeV for this source might be larger) and the flux F_γ observed at energy >0.2 TeV (in $\text{erg cm}^{-2} \text{s}^{-1}$), for blazars observed at different redshift z . The errors indicate the statistical uncertainty; the corresponding systematic uncertainties on the spectral index are typically about 0.1 for H.E.S.S. and about 0.2 for MAGIC. In the column IACT, the Cherenkov telescope with which the data have been collected: symbols stand for H=H.E.S.S., M=MAGIC, V=VERITAS, W=Whipple. In the last column, the references.

strongly flaring (see Fig. 45). The VHE spectrum of 3C 279 has been observed by MAGIC at 6.1σ for energies lower than 220 GeV and at 5.2σ within 220 and 600 GeV [179].

The very well studied sources M 87, Mkn 421, and Mkn 501 (Fig. 46) show a strong temporal variability. These sources, which are monitored by all IACTs, show correlations between TeV and X-ray emission. During the flares, the spectral features change, and the IC peak shifts to higher frequencies (Fig. 46). The highlight of these observations is the detection of very fast (few minutes timescale) variability with some time delay between photons of different energy. Such lags are a potentially powerful diagnostics of acceleration and energy loss processes, whereas the short timescales involved can place tight limits to the size of the emitting regions and the Lorentz factor of the jet. The H.E.S.S. observations of PKS 2155-304 (located at $z=0.116$), showed a very fast flux variability: on the night of July 28 th, 2006 it had a peak flux about 50 times its average flux (and about 15 times the Crab flux), and rapidly doubled it in four successive episodes

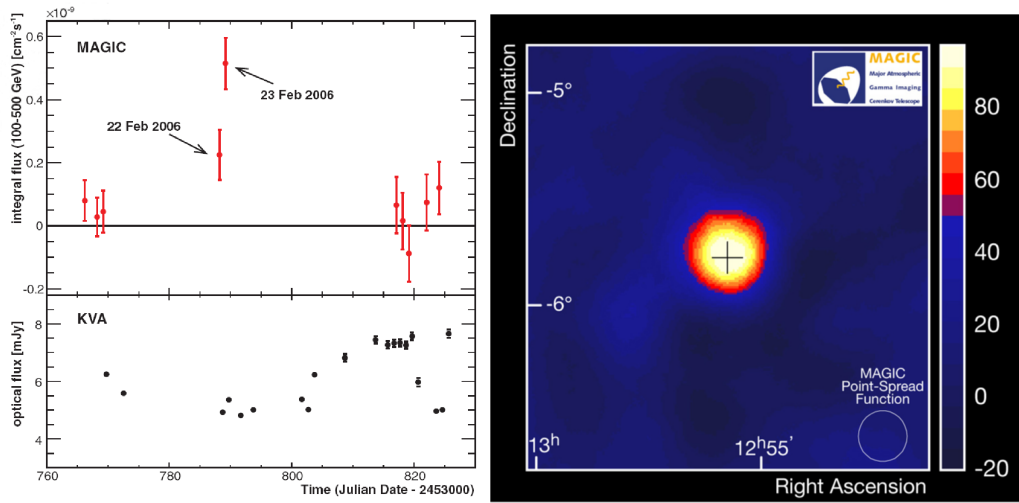


Figure 45. – Lighcurve (left) and skymap on February 23rd, 2006 (right) of 3C 279 [176].

(in 67 ± 50 s, 116 ± 50 s, 173 ± 50 s, and 178 ± 50 s respectively). As for M 87, this source is not a blazar but a radio galaxy that harbors the most massive known black hole in the nearby universe and whose jet is $\sim 30^\circ$ from the line of sight to the observer: hence the two-day timescale measured by H.E.S.S. [178] is remarkable.

The variability of the AGN in the VHE region can provide information about possible violations of the Lorentz invariance by means of the light dispersion expected in some

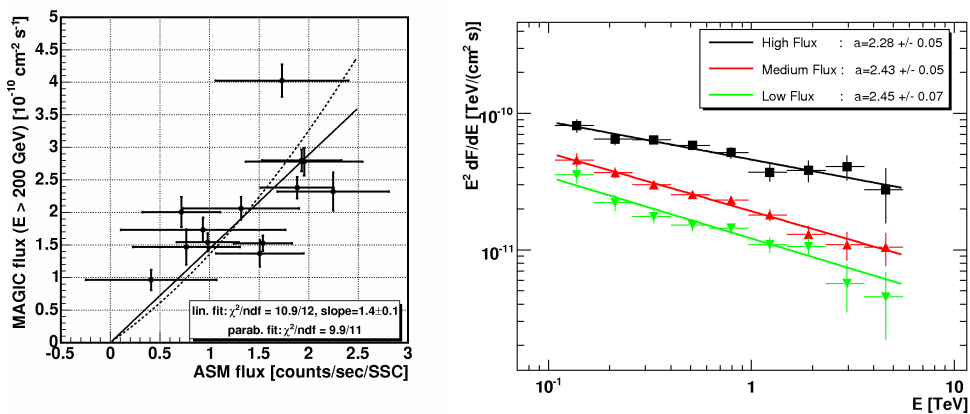


Figure 46. – Left: TeV-X ray correlation for from Mkn 421 [151]. Right: the spectral energy distribution from Mkn 501 [146] during different flares.

quantum gravity models [55]. The velocity of light in such models is given by the formula:

$$V = c \left[1 + \xi \left(\frac{E}{E_{QG}} \right) + \xi_2 \left(\frac{E}{E_{QG}} \right)^2 + \dots \right]$$

where E_{QG} is the energy scale where Lorentz invariance is violated, and the ξ s are parameters of order unity which can be positive or negative. At first order photons of different energies emitted at the same time are detected with a time delay $\Delta t \simeq \xi \frac{E}{E_{QG}} \frac{z}{H_0} = \xi \frac{E}{E_{QG}} \frac{L}{c}$. The MAGIC data about Mkn 501 [180] showed a negative correlation between the arrival time of photons and their energy (Fig. 47), yielding, if one assumes that the delay is due to quantum gravity effects, to an evaluation of $E_{QG} \sim 0.03 M_P$ ($E_{QG} > 0.02 M_P$)⁽⁶⁾. H.E.S.S. observations of PKS 2155 [157] evidenced no effect, allowing to set a lower limit $E_{QG} > 0.04 M_P$; in 1999 Whipple data [181] lead to $E_{QG} > 0.005 M_P$ and the X-ray limits from Gamma-Ray Bursts give $E_{QG} > 0.01 M_P$.

In most quantum gravity scenarios violations to the universality of the speed of light happen at order larger than 1: $\Delta t \simeq (E/E_{QG})^\nu$ with $\nu > 1$. In this case the VHE detectors are even more sensitive with respect to other instruments; for $\nu = 2$ the data from PKS 2155 give $E_{QG} > 3 \cdot 10^{-9} M_P$.

5.2.4. Gamma-Ray Bursts. Gamma-Ray Bursts (GRBs) are widely interpreted as originating in relativistic “fireballs” following the core-collapse of massive stars and/or the coalescence of two compact objects. GRBs are interesting both for astrophysical reasons and related to the physics of photon propagation. At present, no VHE γ -ray emissions from GRBs have been positively detected; the current record of a HE photon is set by EGRET at 18 GeV, two hours after the primary burst.

MAGIC observed part of the prompt-emission phase of GRB 050713a (Fig. 48) as a response to an alert by the Swift satellite [182]. However, no excess at energies larger than 175 GeV was detected, neither during the prompt emission phase nor later – but the upper limits to the MAGIC flux are compatible with simple extrapolations of the power-law spectrum measured by Swift, with spectral index of about 1.6, to hundreds of GeV. In general, however, the cosmological distances of these sources prevent VHE detection [183]: the average redshift of the GRBs for which MAGIC was alerted (and whose z are known) is $\langle z \rangle = 3.22$, whereas at 70 GeV the cosmological γ -ray horizon is $z \sim 1$. Complementary Whipple data [184] and MILAGRO data [185] provide upper limits on, respectively, the late VHE emission (about 4 hours after the burst) from several long-duration GRBs, and on the prompt/delayed emission from several, reputedly nearby ($z \lesssim 0.5$), short-duration GRBs. The “naked-eye” event GRB080319B [186] was unfortunately not observed with MAGIC, in spite of its optimal sky location and relative proximity ($z=0.937$), due to its occurring at twilight, nor with AGILE, due to its being occulted by the Earth at the time of its occurrence.

The MAGIC telescope is at present the best Cherenkov telescope to observe GRBs, due to its fast movement and its low energy threshold; furthermore, MAGIC is in the GCN Network for GRB alerts (see Fig. 49) which is active since April 2005. However,

⁽⁶⁾ Quantum Gravity effects are usually parametrized as a function of the reduced Planck mass M_P , where violations are expected to become sizeable. The reduced Planck mass, $[(\hbar c)(8\pi G)]^{1/2}$, is, apart from factors of order 1, the mass of a black hole whose Schwarzschild radius equals its Compton wavelength.

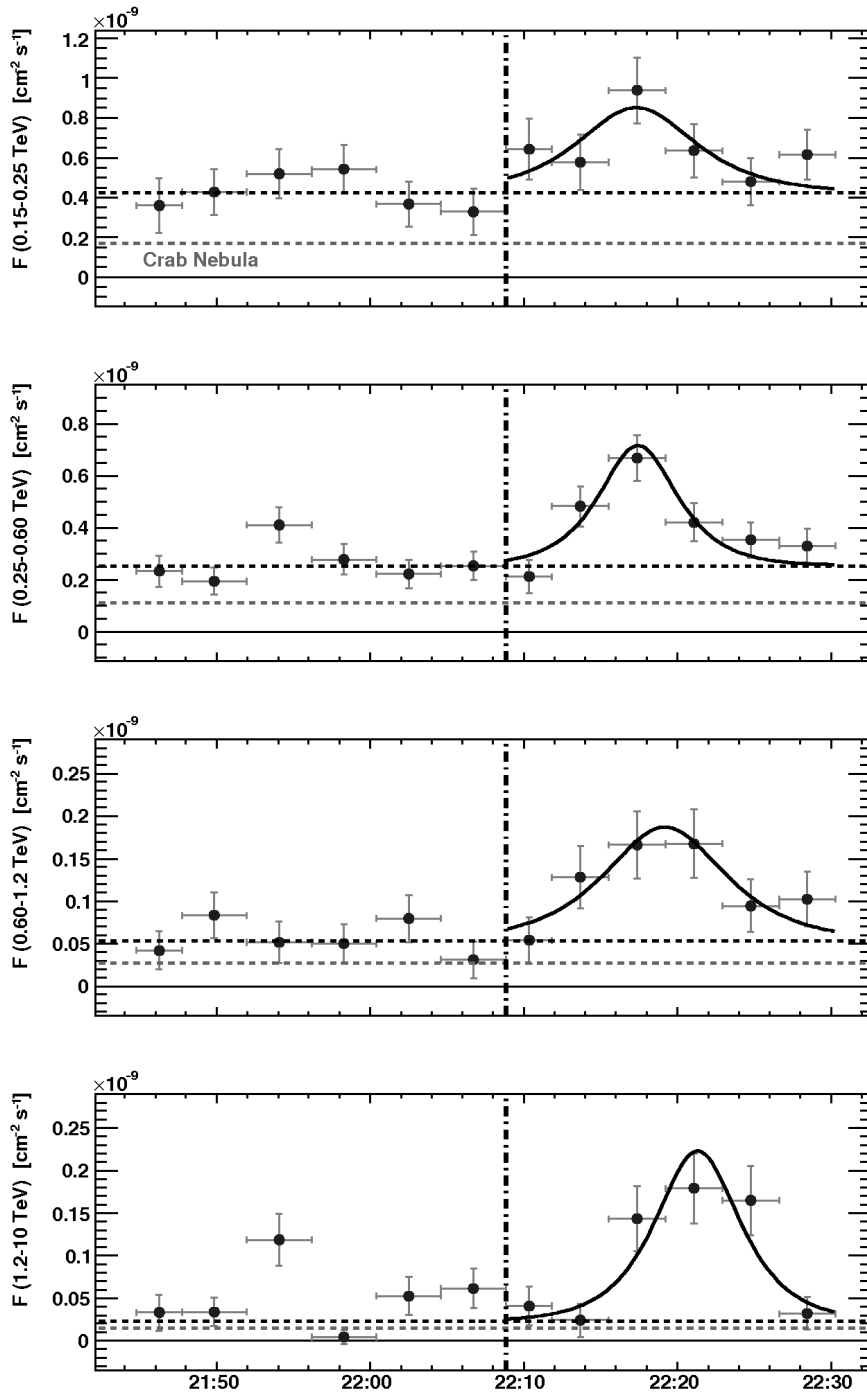


Figure 47. – Integral flux of Mkn 501 detected by MAGIC in four different energy ranges [146].

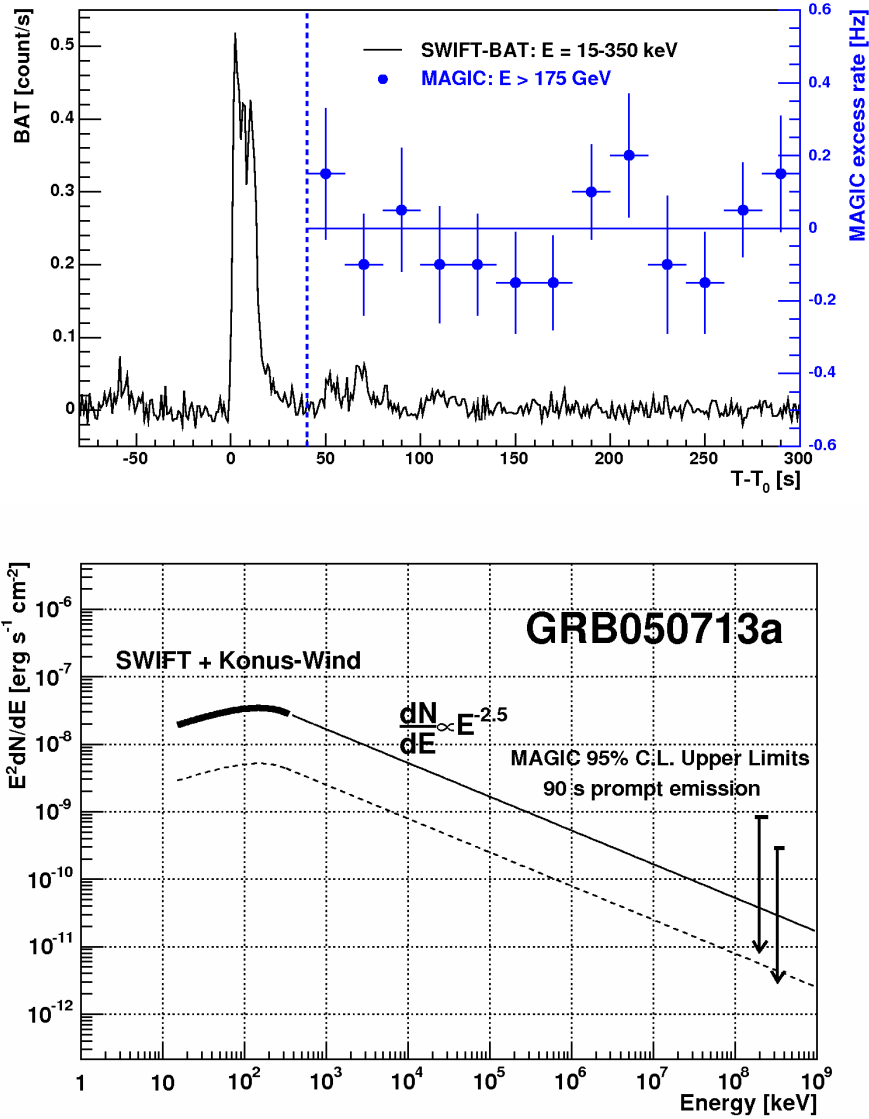


Figure 48. – Plots of the MAGIC data about the GRB 050713a [182]: up, excess event rate compared with SWIFT-BAT observations; down: upper limits on the spectrum.

VHE observations of GRBs are severely limited by EBL absorption: only a small fraction will likely occur at $z < 1$, and these will have to be observed at energies substantially below 100 GeV. The MILAGRO and HAWC telescopes has characteristics suitable to the GRB observation, owing to their very large field of view and $\sim 100\%$ duty cycle.

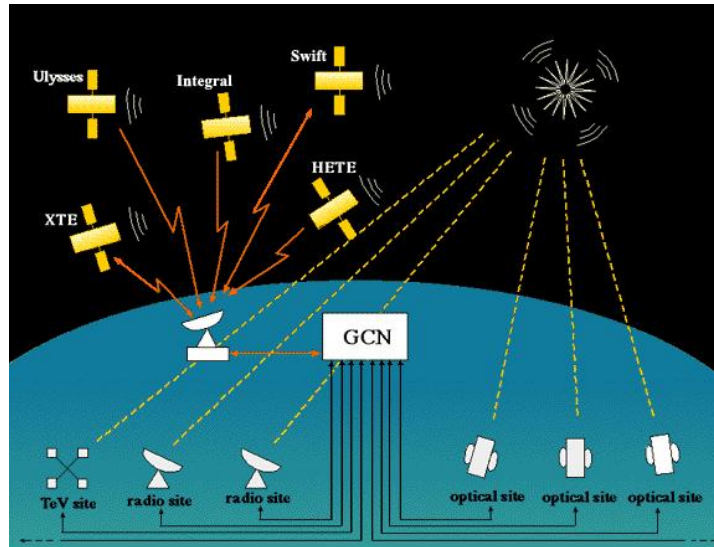


Figure 49. – The GCN Network for GRB alerts [187].

6. – The future

6.1. The future of present detectors. – The next years will be very exciting for the observations of the γ -ray sky. The GLAST satellite telescope is in orbit since June 2008. A second MAGIC telescope, at a distance of 85 m from the first one, starts operating in September 2008 (see Fig. 50); it will increase substantially the sensitivity of MAGIC and improve the angular resolution to about 0.07 degrees. With this new telescope, MAGIC enters in phase 2 (MAGIC 2). The H.E.S.S. collaboration has started the construction of a large telescope, which will be inaugurated after 2009 (see Fig. 50) and will lead the instrument into its phase 2 (H.E.S.S. 2). With its diameter of 28 m, the new telescope, located in the middle of the four existing telescopes, will be the largest Cherenkov telescope in the world, and it should decrease the trigger threshold to some 30 GeV.

What next? Given the present space technology and the progress that one can reasonably foresee, space instruments beyond GLAST are forbidden for the next some 30 years - the cost of space technology forbidding enterprises at a scale one-two orders of magnitude larger than GLAST. The future will then be for ground-based instruments.

When designing a new instrument to detect VHE sources, we must learn from experience. H.E.S.S. and MAGIC have explored with enormous success most of the sky, including the galactic plane and most EGRET sources, and we learned that:

- Extensive Air Shower detectors need to increase their sensitivity by a factor of about 10 to stay in the market; they should become larger and collect a flux of about 1% Crab per year or less;
- to further improve the IACTs, it is needed to build instruments with a larger field of view by using new geometries or by replicating the present Cherenkov instruments, maybe with some improvements such as adopting silicon photomultipliers (cheaper, lighter and smaller, with advantages on the weight and the engineering



Figure 50. – The telescopes MAGIC 2 (real view) [188] and H.E.S.S. 2 (artist view) [189].

of the camera) or adopting new technologies for mirrors. The cost of telescopes is presently dominated by mechanics, mirrors, and camera.

Two longer-term projects for ground telescopes are under discussion: the Cherenkov Telescope Array (CTA) [190], and an EAS detector called High Altitude Water Cherenkov (HAWC) [191].

6.2. The Cherenkov Telescope Array. – The CTA facility is a European project meant to explore the sky in the energy range from 10 GeV to 100 TeV and it is designed to combine guaranteed science with significant discovery potential. It is designed to be built using demonstrated technologies, i.e., being a replica of present Cherenkov telescopes. The CTA is a cornerstone towards a multi-messenger exploration of the universe.

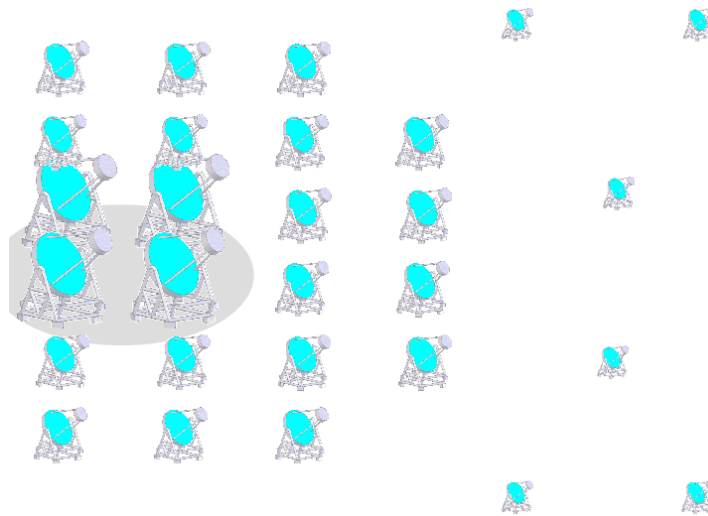


Figure 51. – A possible layout for the CTA [190].

In the most ambitious and expensive scheme, for which the cost foreseen is of the order of 100-150 million euros, the array layout will be composed by 3 zones (see Fig. 51), with different types of telescopes.

- The low-energy section, which is the innermost part, is covered with a sampling of 10% by large telescopes with medium-field cameras; its radius will be about 70 m and its energy threshold will be of about 10 GeV.
- The medium-energy section will be covered with a sampling of 1% by mid-size telescopes; its radius will be 250 m in addition to the low-energy section and its energy threshold will be of about 100 GeV.
- The high-energy section will be covered at 0.05% by small telescopes with wide-field cameras; its radius will be few kilometers in addition to the medium-energy section and its energy threshold will be of about 1 TeV.

The field of view increases from 4-5 degrees in the inner region to 8-10 degrees in the outer sections.

In such a scenario, the CTA will operate in four different modes:

- deep wide-band mode, when all the telescopes track the same source;
- survey mode, when the telescopes survey the sky using a staggered pattern of fields of view;
- search and monitoring mode, when subclusters of telescopes track different sources;
- narrow-band mode, when halo telescopes accumulate high-energy data, while the core telescopes hunt for pulsars.

Two sites are foreseen for the CTA: one in the northern and one in the southern hemisphere.

At the 30th International Cosmic Ray Conference (2007), a board of scientists affiliated to institutions from U.S.A. presented a white paper [192] about the status and the future of ground-based γ -ray astronomy, in which they propose some baselines for the development of the future instruments. In particular, they identify some requirements that the future instruments should meet, among which are the following:

- one order of magnitude better sensitivity by means of a footprint area on the order of 1 km²;
- enlargement of the explored energy range;
- improvement of the angular resolution;
- a factor 2 of increase of the field of view.

The technology they propose is an array of mid-size IACTs (5-15 m diameter) coupled to an array of water Cherenkov detectors, the latter to provide a large field of view and a high duty-cycle. For what concerns the IACTs themselves, they suggest to:

- reduce the construction and operational costs;
- move from the present Davies-Cotton or parabolic optics to Cassegrain optics, in order to increase the field of view;
- design the readout and triggering electronics, choose the photodetector and the mirror fabrication technique in such a way to improve the sensitivity and cut down the expenses.

The future Cherenkov arrays will observe many new sources at low energies, but maybe very exciting new discoveries will come from the few expected new sources in the high energy region, which could generate important new physics.

Finally, research has started for large field-of-view imaging atmospheric Cherenkov telescopes with Fresnel optics [193], which could combine the precision and the sensitivity of IACTs with a field of view as large as 40 degrees.

An intermediate model for the CTA, for which the cost could be dropped to some 20 million euros or less, would be to stage the final detector by building a third MAGIC telescope and several H.E.S.S. 1 detectors, all with advanced high-efficiency cameras. In this case the overall sensitivity would improve by a factor of 2 to 3 instead than the final design factor of 10, but this would give the time to explore the potential of the observations by the joint collaboration with a substantial increase in sensitivity and with limited funding.

6.3. Large EAS. – The High Altitude Water Cherenkov (HAWC) observatory, the successor of MILAGRO, will be located at the extreme altitude of 4 100 m in the Sierra Negra (Mexico). Such an altitude will allow lowering the threshold, by intercepting a larger amount of charged secondaries. It will incorporate new design solutions like placing the photomultipliers in isolated tanks, and adopting a larger spacing between them. It will have a 22 500 m² sensitive area (to be compared with the 4 000 m² of MILAGRO) and since it will reuse in the beginning the MILAGRO photomultipliers and electronics it will cost only about 10 to 20 million dollars to complete the detector (to be compared

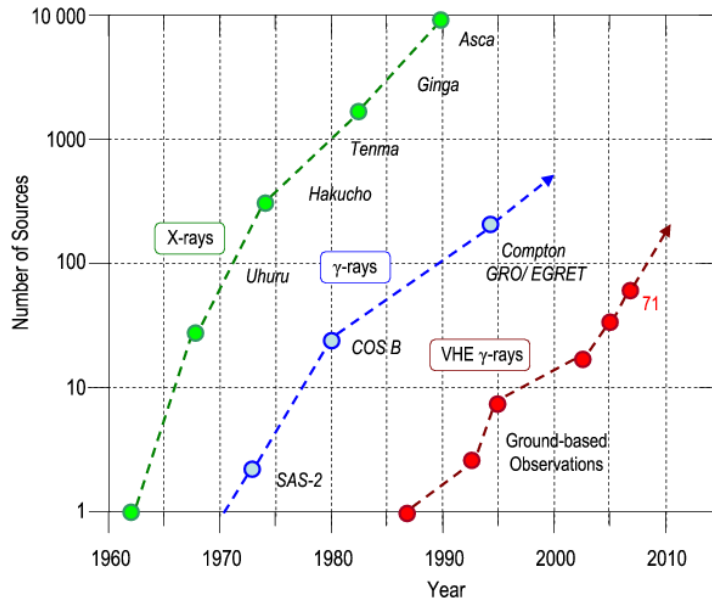


Figure 52. – The “Kifune plot” which shows the number of detected sources as a function of time from year 1960, with an extrapolation to the next future. The plot has been updated in [13].

to the about 150 million euros foreseen for the “full version” of the CTA). HAWC will improve the sensitivity of MILAGRO by at least one order of magnitude: it will detect the Crab Nebula in one day at 5σ and collect four times the Crab flux in 15 minutes, being suitable for γ -ray bursts observations. HAWC will probably have a lower energy threshold at 200 GeV.

The capability of the HAWC observatory to perform a highly sensitive all-sky survey will enable the monitoring of the known sources and yield to the discovery of new sources of known types and new classes of TeV sources. Furthermore, HAWC can investigate the origin and propagation of cosmic rays above the TeV - tens of TeV region.

7. – Conclusions

High-energy photons are a powerful probe of fundamental physics under extreme conditions, since they are produced in the highest energy phenomena, they often travel through large distances, and their interactions display large boosts towards the center of mass.

Observation of X- and γ -rays gives an exciting view of the HE universe thanks to satellite-based telescopes (AGILE, GLAST) and to ground-based detectors like the IACTs, which discovered more than 60 new VHE sources in the last 3 years and are going on this way. This large population of VHE- γ -ray sources, which are often unknown sources, poses questions on the transparency of the Universe at these energy ranges; this might indicate the existence of new physics.

The plot in Fig. 52, usually referred to as “Kifune plot”, shows how the amount of detected X-ray, γ -ray and VHE- γ -ray sources varied and an extrapolation to the future; the contribution from the different observatories is highlighted. In this plot we can see that the advent of the IACTs like MAGIC and H.E.S.S. increased by a factor of 10 the known VHE- γ -ray source population. The progress achieved with the latest generation of IACTs is comparable with the one drawn by EGRET with respect to the previous γ -ray satellite detectors.

This exciting scenario gives handles for the study of new mechanisms about the VHE- γ -ray origin and propagation, and many astrophysical constraints are feeding the theories. So far no clear sources above about 50 TeV have been detected, but it is still uncertain whether they do not exist or there is just a technological limit on detecting them with the current facilities; the future instruments will tell. The exploration of the VHE sources has just started and in the next three years (2008/2010) a factor of 10 improvement in the GeV range is expected by the AGILE and GLAST observations, while a factor 2-3 improvement in the TeV range will be reached by H.E.S.S. 2, MAGIC 2 and VERITAS.

To go beyond the TeV energies the best solution comes from the combination provided by the CTA and HAWC observatories, and possibly from new concepts of large-field of view facilities.

Acknowledgements

The Authors thank Abelardo Moralejo, Barbara De Lotto, Carlotta Pittori, Fabrizio Tavecchio, Florian Göbel, Marco Roncadelli, Robert Wagner for comments and suggestions. A special acknowledgement goes to the anonymous referee who helped in improving the article.

REFERENCES

- [1] V. HESS, *Phys. Z.*, **13** (1913) 1084.
- [2] D. PACINI, *Nuovo Cim.*, **3** (1912) 93.
- [3] B. ROSSI, *High-energy Particles* (Prentice-Hall, New York) 1952;
B. ROSSI, *Cosmic Rays* (McGraw-Hill, New York) 1964.
- [4] K. GREISEN, *Phys. Rev. Lett.*, **16** (1966) 748;
G.T. ZATSEPIN and V.A. KUZMIN, *J. Exp. Theor. Phys. Lett.*, **4** (1966) 78.
- [5] T. YAMAMOTO, FOR THE PIERRE AUGER COLLABORATION, Proc. 30th Intl. Cosmic Ray Conf. (ICRC 2007), in press (arXiv:0707.2638).
- [6] E. FERMI, *Phys. Rev.*, **75** (1949) 1169.
- [7] See, for example, E. ZWIEBEL and C. HEILES, *Nature*, **385** (1997) 131.
- [8] THE PIERRE AUGER COLLABORATION, *Science*, **318** (2007) 938.
- [9] A. DE ANGELIS, M. RONCADELLI and M. PERSIC, *Mod. Phys. Lett. A*, **23** (2008) 315.
- [10] M.T. RESSELL and M.S. TURNER, *Comm. on Astrophys.*, **14** (1990) 323.
- [11] F.A. AHARONIAN, *Very High Energy Cosmic Gamma Radiation* (World Scientific, Singapore) 2004.
- [12] C.M. HOFFMAN, C. SINNIS, P. FLEURY, and M. PUNCH, *Rev. Mod. Phys.*, **71** (1999) 897.
- [13] J. HINTON, Proc. 30th Intl. Cosmic Ray Conf. (ICRC 2007), in press (arXiv:0712.3352).
- [14] J. HINTON, *New J. Phys.*, in press (arXiv:0803.1609).
- [15] T.C. WEEKES ET AL., *Astrophys. J.*, **342** (1989) 379.
- [16] K. MANNHEIM, *Astron. Astrophys.*, **269** (1993) 76.
- [17] F.A. AHARONIAN, *New Astron.*, **5** (2000) 377.
- [18] C.M. URRY and P. PADOVANI, *Publ. Astron. Soc. Pacific*, **107** (1995) 803.

- [19] P. PADOVANI, *Am. Inst. Phys. Conf. Proc.*, **921** (2007) 19.
- [20] M.H. ULRICH ET AL., *Ann. Rev. Astron. Astrophys.*, **35** (1997) 445.
- [21] G. FOSSATI ET AL., *Mon. Not. R. Astron. Soc.*, **299** (1998) 433.
- [22] G. GHISELLINI ET AL., *Mon. Not. R. Astron. Soc.*, **301** (1998) 451.
- [23] C. DERMER and R. SCHLICKEISER, *Astrophys. J.*, **416** (1993) 458.
- [24] M.J. REES, *Mon. Not. R. Astron. Soc.*, **137** (1967) 429.
- [25] L. MARASCHI, G. GHISELLINI, and A. CELOTTI, *Astrophys. J.*, **397** (1992) L5.
- [26] M.J. REES and P. MESZAROS, *Mon. Not. R. Astron. Soc.*, **258** (1992) 41.
- [27] P. MESZAROS and M.J. REES, *Astrophys. J.*, **405** (1993) 278.
- [28] R. SARI ET AL., *Astrophys. J.*, **497** (1998) L17.
- [29] P. MESZAROS, *Rep. Prog. Phys.*, **69** (2006) 2259.
- [30] T.S. VAN ALBADA ET AL., *Astrophys. J.*, **295** (1985) 305.
- [31] C. SARAZIN, *Rev. Mod. Phys.*, **58** (1986) 1.
- [32] D.N. SPERGEL ET AL., *Astrophys. J. Suppl.*, **148** (2003) 175.
- [33] W.-M. YAO ET AL., *J. Phys.*, **G33** (2006) 1 and 2007 partial update for 2008.
- [34] *GLAST Science Brochure (March 2001)*, <http://glast.gsfc.nasa.gov/science>.
- [35] T. BRINGMANN, L. BERGSTRÖM, and J. EDSJÖ, *J. High Energy Phys.*, **01** (2007) 049.
- [36] F.A. AHARONIAN ET AL., *Nature*, **439** (2006) 695.
- [37] P. COPPI and F.A. AHARONIAN, *Astrophys. J.*, **487** (1997) L9.
- [38] W. HEITLER, *The quantum theory of radiation* (Oxford University Press, Oxford) 1960.
- [39] S. LEE, *Phys. Rev. D*, **58** (1998) 043004.
- [40] R.J. GOULD and G.P. SCHRÉDER, *Phys. Rev.*, **155** (1967) 1408.
- [41] F.W. STECKER, *Int. Astron. Union Symp.*, **204** (2001) 135.
- [42] F.W. STECKER, O.C. DE JAGER, and M.H. SALOMON, *Astrophys. J.*, **390** (1992) L49.
- [43] F.A. AHARONIAN ET AL., *Nature*, **440** (2006) 1018.
- [44] D. MAZIN and M. RAUE, *Astron. Astrophys.*, **471** (2007) 439.
- [45] P.J.E. PEEBLES, *Principles of Physical Cosmology* (Princeton University Press, Princeton) 1993.
- [46] T. PADMANABHAN, *Theoretical Astrophysics, Volume III: Galaxies and Cosmology* (Cambridge University Press, Cambridge) 2002.
- [47] O. BLANCH, J. LOPEZ, and M. MARTINEZ, *Astropart. Phys.*, **19** (2003) 245;
O. BLANCH and M. MARTINEZ, *Astropart. Phys.*, **23** (2005) 588;
O. BLANCH and M. MARTINEZ, *Astropart. Phys.*, **23** (2005) 598;
O. BLANCH and M. MARTINEZ, *Astropart. Phys.*, **23** (2005) 608.
- [48] K. MANNHEIM, *Rev. Mod. Astron.*, **12** (1999) 167.
- [49] J.R. PRIMACK ET AL., *Astropart. Phys.*, **11** (1999) 93;
J.R. PRIMACK ET AL., *AIP Conference Proceedings*, **558** (2001) 463.
- [50] A. DE ANGELIS, O. MANSUTTI, and M. RONCADELLI, *Phys. Lett. B*, **659** (2008) 847.
- [51] A. DE ANGELIS, M. RONCADELLI, and O. MANSUTTI, *Phys. Rev. D*, **76** (2007) 121301.
- [52] M. SIMET, D. HOOPER, P. SERPICO, *Phys. Rev. D*, **77** (2008) 063001.
- [53] T.M. KNEISKE ET AL., *Astron. Astrophys.*, **413** (2004) 807.
- [54] T. KIFUNE, *Astrophys. J.*, **518** (1999) L21.
- [55] G. AMELINO-CAMELIA ET AL., *Nature*, **393** (1998) 763.
- [56] A. DE ANGELIS and L. PERUZZO, *Sterne Weltraum*, **8** (2007) 26.
- [57] B. ROSSI, K. GREISEN, *Rev. Mod. Phys.*, **13** (1941) 240.
- [58] J. NISHIMURA, K. KAMATA, *Prog. Theor. Phys.*, **7** (1952) 185;
K. GREISEN, *Rev. Mod. Phys.*, **13** (1960) 240.
- [59] R.M. WAGNER, Ph.D. thesis, 2006, Technische Universität München, MPP-2006-245.
- [60] *GLAST Gallery*, <http://www-glast.sonoma.edu/resources/multimedia/gallery/>.
- [61] *CGRO Science Support Center Image Gallery*,
<http://coss.gsfc.nasa.gov/docs/cgro/images/epo/gallery/glast/>.
- [62] *AGILE, Astro-rivelatore Gamma a Immagini Leggero*, <http://agile.asdc.asi.it/>.
- [63] GODDARD SPACE FLIGHT CENTER, NASA, *The GLAST Instruments*,
<http://glast.gsfc.nasa.gov/public/instruments.html>.

- [64] GODDARD SPACE FLIGHT CENTER NEWS, NASA,
http://www.nasa.gov/centers/goddard/news/topstory/2007/GlastLaunch_prt.htm.
- [65] STANFORD LINEAR ACCELERATOR CENTER, *GLAST LAT Performance*,
<http://www-glast.slac.stanford.edu/software/IS/>.
- [66] THE MILAGRO GAMMA-RAY OBSERVATORY, LANL, *The Detection of Cosmic Rays*,
<http://www.lanl.gov/milagro/detecting.shtml>
- [67] INFN ROMA 3, *The Argo-YBJ Experiment*,
<http://193.204.162.110/~nucleare/argo/argo.html>.
- [68] THE MILAGRO GAMMA-RAY OBSERVATORY, LANL, <http://www.lanl.gov/milagro/>.
- [69] A.M. HILLAS, Proc. 19th Intl. Cosmic Ray Conf. (ICRC 1985);
A.M. HILLAS, *Space Sci. Rev.*, **75** (1996) 17.
- [70] F. PIRON ET AL., *Astron. Astrophys.*, **374** (2001) 895;
M. DE NAUROIS, arXiv:astro-ph/0607247v1;
M. LEMOINE-GOUMARD, B. DEGRANGE, and M. TLUCZYKONT, *Astropart. Phys.*, **25** (2006) 195.
- [71] D. BERGE, S. FUNK, and J. HINTON, *Astron. Astrophys.*, **466** (2007) 1219.
- [72] V.R. CHITNIS and P.N. BHAT, *Astropart. Phys.*, **15** (2001) 29;
S. RADUCCI, Thesis at the Università di Udine, 2004;
D. TESCARO, Thesis at the Università di Padova, 2005;
R. MIRZOYAN ET AL., *Astropart. Phys.*, **25** (2006) 342;
D. TESCARO ET AL., arXiv:0709.1410v1 [astro-ph];
G. CABRAS ET AL., arXiv:0804.3896v1 [astro-ph].
- [73] MAX PLANCK INSTITUTE, *The H.E.S.S. Telescopes*,
http://www.mpi-hd.mpg.de/hfm/HESS/public/telescope/hn_telescopes.htm.
- [74] UNIVERSITY OF HAMBURG, *H.E.S.S. overview*,
http://www-hess.desy.de/pages/hes_overview.html.
- [75] MAX-PLANCK-INSTITUT FÜR PHYSIK, MUNICH, *MAGIC Picture Gallery*,
<http://wwwmagic.mppmu.mpg.de/gallery/>.
- [76] *VERITAS Homepage*, <http://veritas.sao.arizona.edu>.
- [77] A. MORALEJO, private communication.
- [78] D. BASTIERI ET AL., *Astropart. Phys.*, **23** (2005) 572
- [79] INSTITUT FÜR THEORETISCHE PHYSIK UND ASTROPHYSIK, FAKULTÄT FÜR PHYSIK UND ASTRONOMIE, UNIVERSITÄT WÜRZBURG, *Observations with the MAGIC Telescope*,
<http://www.astro.uni-wuerzburg.de/mphysics/>.
- [80] http://coss.c.gsfc.nasa.gov/docs/cgro/coss/egret/3rd_EGRET_Cat.html
or Ref. [142].
- [81] <http://www.mppmu.mpg.de/~rwagner/sources/>.
- [82] F.A. AHARONIAN ET AL., *Astrophys. J.*, **636** (2006) 777.
- [83] S. HOPPE ET AL., Proc. 30th Intl. Cosmic Ray Conf. (ICRC 2007), in press (arXiv:0710.3528).
- [84] J. ALBERT ET AL., *Astrophys. J.*, **664** (2006) L87.
- [85] D.F. TORRES ET AL., *Phys. Rep.*, **382** (2003) 303.
- [86] T.A. PORTER ET AL., *Astrophys. J.*, **648** (2006) L29.
- [87] F.A. AHARONIAN ET AL., *Astron. Astrophys.*, **449** (2006) 223.
- [88] E.G. BEREZHKO and H.J. VÖLK, *Astron. Astrophys.*, **451** (2006) 98.
- [89] E.G. BEREZHKO ET AL., *Astron. Astrophys.*, **400** (2003) 971.
- [90] J. ALBERT ET AL., *Astron. Astrophys.*, **474** (2007) 937.
- [91] M. PERSIC, A. DE ANGELIS, F. LONGO, and M. TAVANI, Proc. 30th Intl. Cosmic Ray Conf. (ICRC 2007), in press (arXiv:0709.1881).
- [92] F.A. AHARONIAN ET AL., *Astron. Astrophys.*, **464** (2007) 235.
- [93] P. BLASI, *Mod. Phys. Lett.*, **A20** (2005) 3055.
- [94] J. ALBERT ET AL., *Astrophys. J.*, **643** (2006) L53.
- [95] J. ALBERT ET AL., *Astrophys. J.*, **664** (2007) L87.
- [96] F. AHARONIAN ET AL., *Astron. Astrophys.*, **481** (2008) 401.
- [97] F. PACINI, *Nature*, **216** (1967) 567.

- [98] K.S. CHENG ET AL., *Astrophys. J.*, **300** (1986) 500.
- [99] R.W. ROMANI, *Astrophys. J.*, **470** (1996) 469.
- [100] K. HIROTANI, *Adv. Space Res.*, **35** (2005) 1085.
- [101] J.K. DAUGHERTY and A. HARDING, *Astrophys. J.*, **252** (1982) 337;
J.K. DAUGHERTY and A. HARDING, *Astrophys. J.*, **458** (1996) 278.
- [102] M.G. BARING, *Adv. Space Res.*, **33** (2004) 552.
- [103] F.A. AHARONIAN ET AL., *Astron. Astrophys.*, **448** (2006) L43.
- [104] J. ALBERT ET AL., *Astrophys. J.*, **669** (2007) 1143.
- [105] A.K. HARDING, V.V. USOV, and A. G. MUSLIMOV, *Astrophys. J.*, **622** (2005) 531.
- [106] J. ALBERT ET AL., *Astrophys. J.*, **674** (2008) 1046.
- [107] M. TESHIMA FOR THE MAGIC COLLABORATION, *ATel*, **1491** (2008).
- [108] Y. GALLANT, *Astrophys. Space Sci.*, **309** (2007) 197.
- [109] S. FUNK ET AL., *Astrophys. J.*, **662** (2007) 517.
- [110] S. FUNK ET AL., *Astron. Astrophys.*, **470** (2007) 249.
- [111] D.J. HELFAND, R.H. BECKER, and R.L. WHITE, arXiv:astro-ph/0505392;
C.L. BROGAN ET AL., *Astrophys. J.*, **629** (2005) L105;
D.J. HELFAND ET AL., *Astrophys. J.*, **665** (2007) 1297.
- [112] F.A. AHARONIAN ET AL., *Astron. Astrophys.*, **460** (2006) 365.
- [113] F.A. AHARONIAN ET AL., *Astron. Astrophys.*, **442** (2005) 1.
- [114] F.A. AHARONIAN ET AL., *Science*, **309** (2005) 746.
- [115] F.A. AHARONIAN ET AL., *Astron. Astrophys.*, **460** (2006) 743.
- [116] J. ALBERT ET AL., *Science*, **312** (2006) 1771.
- [117] J. ALBERT ET AL., *Astrophys. J.*, **665** (2007) L51.
- [118] F.A. AHARONIAN ET AL., *Astron. Astrophys.*, **425** (2004) L13.
- [119] J. ALBERT ET AL., *Astrophys. J.*, **638** (2006) L101.
- [120] F.A. AHARONIAN ET AL., *Phys. Rev. Lett.*, **97** (2006) 221102.
- [121] F.A. AHARONIAN ET AL., *Science*, **307** (2005) 1938.
- [122] A. KONOPELKO ET AL., *Astrophys. J.*, **658** (2007) 1062.
- [123] J. ALBERT ET AL., *Astrophys. J.*, **675** (2008) L25.
- [124] F.A. AHARONIAN ET AL., *Astron. Astrophys.*, **431** (2005) 197.
- [125] A. ABDO ET AL., *Astrophys. J.*, **658** (2007) L33;
A. ABDO ET AL., *Astrophys. J.*, **664** (2007) L91.
- [126] M. AMENOMORI ET AL., Proc. 30th Intl. Cosmic Ray Conf. (ICRC 2007), in press (arXiv:0710.2757).
- [127] *H.E.S.S. Source of the Month, August 2007: Confirming MGRO 1908+06*,
http://www.mpi-hd.mpg.de/hfm/HESS/public/som/Som_8_07.htm.
- [128] M. SALVATI, B. SACCO, *Astron. Astrophys.*, **485** (2006) 2008.
- [129] L. DRURY, F.A. AHARONIAN, *Astropart. Phys.* (2008), in press (arXiv:0802.4403).
- [130] L. BERGSTRÖM and D. HOOPER, *Phys. Rev. D*, **73** (2006) 063510.
- [131] J. ALBERT ET AL., *Astrophys. J.*, **679** (2008) 428.
- [132] C. ITOH ET AL., *Astron. Astrophys.*, **462** (2007) 67.
- [133] A.W. STRONG ET AL., *Astrophys. J.*, **537** (2000) 763.
- [134] D.F. TORRES, *Astrophys. J.*, **617** (2004) 966.
- [135] H. VÖLK ET AL., *Space Sci. Rev.*, **75** (1996) 279.
- [136] T.A.D. PAGLIONE ET AL., *Astrophys. J.*, **460** (1996) 295.
- [137] E. DOMINGO-SANTAMARÍA and D. TORRES, *Astron. Astrophys.*, **444** (2005) 403.
- [138] F.A. AHARONIAN ET AL., *Astron. Astrophys.*, **442** (2005) 177.
- [139] J. ALBERT ET AL., *Astrophys. J.*, **658** (2007) 245.
- [140] F. TAVECCHIO ET AL., *Astrophys. J.*, **509** (1998) 608.
- [141] M. PERSIC, Y. REPHAELI, and Y. ARIELI, *Astron. Astrophys.* (2008), in press (arXiv:0802.0818).
- [142] R.C. HARTMAN, *Astrophys. J. Suppl.*, **123** (1999) 79.
- [143] M. PUNCH ET AL., *Nature*, **358** (1992) 477.
- [144] M. PERSIC and A. DE ANGELIS, *Astron. Astrophys.*, **483** (2008) 1.
- [145] E. PIAN ET AL., *Astrophys. J.*, **492** (1998) L17.

- [146] J. ALBERT ET AL., *Astrophys. J.*, **669** (2007) 862.
- [147] G.G. FAZIO and F. W. STECKER, *Nature*, **226** (1970) 135.
- [148] O.C. DE JAGER and F. W. STECKER, *Astrophys. J.*, **566** (2002) 738.
- [149] D. MAZIN and F. GOEBEL, *Astrophys. J.*, **655** (2007) L13.
- [150] F. AHARONIAN ET AL., *Astron. Astrophys.*, **403** (2003) L1.
- [151] J. ALBERT ET AL., *Astrophys. J.*, **663** (2007) 125.
- [152] J. ALBERT ET AL., *Astrophys. J.*, **662** (2007) 892.
- [153] J. ALBERT ET AL., *Astrophys. J.*, **648** (2006) L105.
- [154] J. ALBERT ET AL., *Astrophys. J.*, **639** (2006) 761.
- [155] J. ALBERT ET AL., *Astrophys. J.*, **666** (2007) L17.
- [156] G. SUPERINA ET AL., Proc. 30th Intl. Cosmic Ray Conf. (ICRC 2007), in press (arXiv:0710.4057, 138).
- [157] F.A. AHARONIAN ET AL., *Astron. Astrophys.*, **442** (2005) 895.
- [158] E.S. PERLMAN ET AL., *Astrophys. J.*, **523** (1999) L11.
- [159] F.A. AHARONIAN ET AL., *Astron. Astrophys.* (2008), in press (arXiv:0802.4021v2).
- [160] D. DONATO ET AL., *Astron. Astrophys.*, **375** (2001) 739.
- [161] S. SWORDY FOR THE VERITAS COLLABORATION, *ATel*, **1422** (2008).
- [162] F.A. AHARONIAN ET AL., *Astron. Astrophys.*, **436** (2005) L17.
- [163] D. HORAN ET AL., *Astrophys. J.*, **571** (2002) 753.
- [164] R.M. SAMBRUNA ET AL., *Astrophys. J.*, **483** (1997) 774.
- [165] S. SWORDY FOR THE VERITAS COLLABORATION, *ATel*, **1415** (2008).
- [166] F.A. AHARONIAN ET AL., *Astron. Astrophys.*, **475** (2007) L9.
- [167] E.S. PERLMAN ET AL., *strophys. J. S.*, **104** (1996) 251.
- [168] D. DONATO, R.M. SAMBRUNA, and M. GLIOZZI, *Astron. Astrophys.*, **433** (2005) 1163.
- [169] F.A. AHARONIAN ET AL., *Astron. Astrophys.*, **455** (2006) 461.
- [170] K.S. WOOD ET AL., *Astrophys. J. S.*, **56** (1984) 507.
- [171] J. ALBERT ET AL., *Astrophys. J.*, **642** (2006) L119.
- [172] F.A. AHARONIAN ET AL., *Astron. Astrophys.*, **470** (2007) 475.
- [173] F.A. AHARONIAN ET AL., *Astron. Astrophys.*, **473** (2007) L25.
- [174] J. ALBERT ET AL., *Astrophys. J.*, **667** (2007) L21.
- [175] J. ALBERT ET AL., *Astrophys. J.*, **654** (2007) L119.
- [176] J. ALBERT ET AL., *Science*, **320** (2008) 1752.
- [177] M. TESHIMA FOR THE MAGIC COLLABORATION, *ATel*, **1500** (2008).
- [178] J.-PH. LENAIN, *Rev. Mex. A. A.*, in press (arXiv:0709.1366).
- [179] M. TESHIMA ET AL., Proc. of the 30th International Cosmic Ray Conference (ICRC 2007), arXiv:0709.1475v1 [astro-ph].
- [180] J. ALBERT ET AL., *Phys. Lett. B*, submitted (arXiv:0708.2889).
- [181] S.D. BILLER ET AL., *Phys. Rev. Lett.*, **83** (1999) 2108.
- [182] J. ALBERT ET AL., *Astrophys. J.*, **641** (2006) L9.
- [183] J. ALBERT ET AL., *Astrophys. J.*, **667** (2007) 358.
- [184] D. HORAN ET AL., *Astrophys. J.*, **655** (2007) 396.
- [185] A.A. ABDO ET AL., *Astrophys. J.*, **666** (2007) 361.
- [186] J.S. BLOOM ET AL., *Astrophys. J.* (2008), in press (arXiv:0803.3215).
- [187] GODDARD SPACE FLIGHT CENTER, NASA, *GCN: The Gamma-ray bursts Coordinates Network*, <http://gcn.gsfc.nasa.gov/>.
- [188] *MAGIC picture gallery*, <http://www.magic.mppmu.mpg.de/gallery/pictures/>.
- [189] D. HORNS, *J. Phys.: Conf. Ser.*, **60** (2007) 119.
- [190] <http://www.mpi-hd.mpg.de/hfm/CTA/>.
- [191] See for example: A.J. SMITH, *J. Phys.*, **60** (2007) 131.
- [192] H. KRAWCZYNSKI ET AL. FOR THE WHITE PAPER TEAM, Proc. of the 30th Intl. Cosmic Ray Conf. (ICRC 2007), in press (arXiv:0709.0704).
- [193] G. CUSUMANO ET AL., Proc. of the 30th Intl. Cosmic Ray Conf. (ICRC 2007), in press (arXiv:0707.4541).